# Biomolecule-assisted exfoliation and dispersion of graphene and other two-dimensional materials: a review of recent progress and applications

J.I. Paredes*, S. Villar-Rodil

*Instituto Nacional del Carbón, INCAR-CSIC, Apartado 73, 33080 Oviedo, Spain*

*Corresponding author: paredes@incar.csic.es

**Abstract**

Direct liquid-phase exfoliation of layered materials by means of ultrasound, shear forces or electrochemical intercalation holds enormous promise as a convenient, cost-effective approach towards the mass production of two-dimensional (2D) materials, particularly in the form of colloidal suspensions of high quality, micrometer- and submicrometer-sized flakes. Of special relevance due to environmental and practical reasons is the production of 2D materials in aqueous medium, which generally requires the use of certain additives (surfactants and other types of dispersants) to assist in the exfoliation and colloidal stabilization processes. In this context, biomolecules have received in recent years increasing attention as dispersants for 2D materials, as they provide a number of advantages over more conventional, synthetic surfactants. Here, we review the research progress in the use of biomolecules as exfoliating and dispersing agents for the production of 2D materials. Although most efforts in this area have focused on graphene, significant advances have also been reported with transition metal dichalcogenides ($MoS_2$, $WS_2$, etc) or hexagonal boron nitride. Particular emphasis is placed on the specific merits of different types of biomolecules, including proteins and peptides, nucleotides and nucleic acids (RNA, DNA), polysaccharides, plant extracts and bile salts, in their role as efficient colloidal dispersants of 2D materials, as well as on the potential applications that have been explored for such biomolecule-exfoliated materials. These applications are wide-ranging and encompass the fields of biomedicine (photothermal and photodynamic therapy, bioimaging, biosensing, etc), energy storage (Li- and Na-ion batteries), catalysis (e.g., catalyst supports for the oxygen reduction reaction or electrocatalysts for the hydrogen evolution reaction), or composite materials. As an incipient area of research, a number of knowledge gaps, unresolved issues and

novel future directions remain to be addressed for biomolecule-exfoliated 2D materials, which will be discussed in the last part of this review.

## 1. Introduction

Owing to their promise as key players in the development of future disruptive technologies, graphene and other two-dimensional (2D) materials, including layered transition metal dichalcogenides (TMDs; e.g. $MoS_2$ or $WS_2$) and transition metal oxides (TMOs; e.g., $MnO_2$ or $WO_3$), hexagonal boron nitride (h-BN), phosphorene or silicene, are currently the focus of extensive and concerted research efforts worldwide.[1–3] At the heart of this strong interest in single- and few-layer sheets of such materials lie a number of exceptional physical properties (e.g., electronic, mechanical, thermal and/or optical) that are frequently absent from their corresponding three-dimensional layered counterparts and only arise as a result of their reduced dimensionality.[4] Thus, the wide diversity of 2D materials in terms of both properties and composition is expected to make for a significant impact in many critical technological areas, such as electronics,[5] photonics,[6] energy conversion/storage,[7] biomedicine,[8,9] chemical sensing/biosensing[10,11] or (photo)catalysis.[12]

To come up to the high expectations placed on graphene and other 2D materials, methods for their mass production must be first developed. Ideally, such methods should be cost-effective, easy to implement and scale-up, as well as versatile enough to afford 2D materials with characteristics specifically targeted to each intended application. However, a decade of research into graphene production has taught us that no single method can fulfil all these requirements, and instead we have to resort to a pool of different bottom-up and top-down approaches, each of which having its own advantages and drawbacks.[2,13] Among bottom-up methods, chemical vapor deposition

(CVD), which relies on the reaction of certain organic or inorganic precursors on catalytic (metallic) substrates, is widely touted as a serious contender in the race to mass-produce large-area, high quality wafers of graphene or TMDs suitable for high-end applications in, e.g., electronics or photonics.[14,15] Nevertheless, the CVD process is currently limited by the need of using high temperatures and vacuum, as well as by the subsequent transfer of the wafers to appropriate target substrates that tends to introduce impurities and defects, thus impairing their performance.[14]

Top-down production approaches, on the other hand, rest upon the exfoliation of bulk layered solids to give single- and/or few-layer flakes of the corresponding 2D materials. Of particular relevance are those methods based on direct exfoliation in the liquid phase that typically make use of ultrasound, [4,16] shear forces[17] or electrochemical intercalation[18] to break the constituting layers of the bulk solid apart. Such a strategy is generally able to afford large quantities of high quality flakes of many 2D materials in colloidal dispersion that can be readily processed into coatings or thin films, or combined with other materials to give composites and hybrid systems suitable for different practical uses. Even though direct liquid-phase exfoliation suffers from some drawbacks, most notably low exfoliation yield and polydispersity in flake size and thickness (including low fraction of single-layer flakes),[4,16] its simplicity and versatility makes it extremely attractive in many prospective technological applications. For instance, the exfoliated flakes can be used as fillers in mechanically reinforced and/or electrically conductive composites, components for low-cost solution-printed electronic devices, drug delivery vehicles, catalysts and catalyst supports or electrodes for supercapacitors and Li-ion batteries.[2,4,16] Likewise, this type of wet direct exfoliation has to be contrasted with chemical exfoliation, which involves modification of the starting layered material by some appropriate means so as to facilitate its efficient

cleavage. Prominent examples are the oxidation of graphite to afford graphene oxide and reduced graphene oxide,[19,20], or the intercalation of 2H-phase $MoS_2$ and other TMDs with Li to give single-layer 1T- or 1T′-phase flakes of the corresponding material.[21,22] Although these chemically exfoliated materials boast some attractive features of their own that are important in practical applications,[23–28] the processes required to prepare them usually entail a significant structural alteration of the original layered material (e.g., introduction of defects) that is difficult to fully revert,[29] which in turn limits their scope of application. By contrast, direct exfoliation is known to generally preserve the original structure of the layered material, avoiding the introduction of significant amounts of defects aside from those associated to the presence of edges in the 2D flakes.[4,16]

Research carried out since 2008 has revealed that graphene and other 2D materials can be readily obtained by wet direct exfoliation in some selected (typically high boiling point) organic solvents.[30–32] Alternatively, exfoliation and dispersion can also be accomplished either in ionic liquids[33] or in water.[16] Working in aqueous medium is generally advantageous in terms of production safety, handleability and applicability (e.g., in biomedicine) of these materials.[8,16] Nonetheless many 2D materials, including graphene, TMDs or h-BN are intrinsically hydrophobic in their pristine form, implying that certain stabilizers or surfactants must be used to afford their direct exfoliation and subsequent dispersion in water. Over the last years, a variety of both ionic[34] and non-ionic[34–38] surfactants have been successfully employed towards this end. However, most of these surfactants were of synthetic origin, which raises concerns as regards the cost, environmental impact, toxicity or biocompatibility of the resulting 2D materials.

To help broaden the applicability of 2D materials obtained by direct liquid –phase exfoliation, recent research efforts have explored the use of natural (i.e., biomolecule-

based) stabilizers rather than synthetic ones. Potential benefits of biomolecule-assisted exfoliation include a wide availability of many suitable biomolecules, greater sustainability/environmental friendliness of the production process, better biocompatibility of the exfoliated flakes,[39] as well as inherent (non-covalent) functionalization of the flakes with the biomolecules, which could serve as a chemical handle for further derivatization towards different practical purposes. Progress in this area has been rapid over the last 2–3 years and has encompassed a wide variety of biomolecules (proteins/peptides, nucleotides/DNA, polysaccharides, bile salts, etc). Here, we provide an up-to-date overview of this topic with a focus on (1) the specific merits of the different types of biomolecules that enable them to act as efficient dispersants of 2D materials and (2) the various applications that have been explored for such biomolecule-exfoliated 2D materials. In line with its status as the most intensively investigated of all 2D materials, graphene has received the lion´s share of attention from researchers on this topic, although significant work with $MoS_2$, $WS_2$ or h-BN has also been reported. Finally, we bring this review to a close with a perspective on some of the challenges that need to be addressed in this research area.

## 2. Biomolecule-assisted exfoliation and dispersion of 2D materials

Many relevant layered materials (e.g., graphite, TMDs or h-BN) as well as the high quality single- and few-layer flakes that can be exfoliated from them exhibit a strong hydrophobic character. As a result, the direct exfoliation and dispersion processes that allow the production of such flakes (e.g., by means of ultrasound or shear forces) cannot be accomplished in water unless some appropriate additive (stabilizer) is included.[16] Broadly speaking, for a given substance to be successful as a colloidal stabilizer of a hydrophobic nanomaterial in water, it needs to exhibit an amphiphilic character. Thus,

the hydrophobic section(s) of the amphiphile can readily adsorb onto the surface of the nanomaterial, whereas its hydrophilic components, having a polar and/or ionic nature, are able to extend into and strongly interact with the aqueous medium, furnishing the nanomaterial with colloidal stability by virtue of steric or electrostatic repulsion.[40] This key observation can be used as a general guide in the selection and testing of efficient biomolecules towards the exfoliation and dispersion of 2D materials. In the following, we discuss the research work carried out on this topic according to the specific types of biomolecules that have been explored. Prospective technological uses of the biomolecule-exfoliated 2D materials are also examined in each case. For obvious reasons, the approach to 2D materials contemplated here naturally lends itself to its implementation in biomedical applications (drug delivery, biosensors, tissue engineering scaffolds, etc). Many of the prospective applications that have been reported for biomolecule-exfoliated 2D materials are indeed bio-related, although other areas (energy, catalysis, composite materials, etc) have also been explored.

### *2.1 Proteins and peptides*

Peptides and proteins are biomolecules formed by the assembly of amino acid residues, the main difference between the two lying in the length of the amino acid sequence: peptides are short sequences, whereas proteins are made up of much longer sequences. In their aqueous native state, proteins take on well-defined spatial conformations, whereby certain residues are exposed on the outer surface of the biomolecule and others are confined within the molecular core so as to minimize its solvation free energy. Because the physicochemical characteristics of the residues can be quite diverse depending on its specific type [e.g. the residue can have anionic (acid), cationic (basic), polar nonionic or hydrophobic character], the resulting

peptides/proteins typically exhibit combinations of hydrophilic and hydrophobic segments that make them potentially useful as amphiphilic dispersants for the exfoliation and colloidal stabilization of graphene and other 2D materials. Some proteins and peptides had been previously used for the debundling and subsequent dispersion of 1D carbon nanotubes (CNTs),[41-43] suggesting that they could also be effective in the case of graphene. However, in addition to chemical composition, dimensionality can also be expected to play a role in the propensity of a nanostructured material to be exfoliated and stabilized by a given dispersant, especially if the latter is a bulky molecule, such as a protein or a nucleic acid, that exhibits an intricate structure determined by a delicate balance of intramolecular forces. For example, while nucleic acids have been suggested to wrap around CNTs in a helical fashion,[44] such conformation is not expected to be in place in the stabilization of 2D materials. Very preliminary work with bovine serum albumin (BSA) indicated that the attainment of protein-exfoliated graphene was feasible.[45] As a result, comprehensive studies aimed specifically at 2D materials were then undertaken.

Early work by Laaksonen and co-workers identified a special class of proteins, referred to as hydrophobins, as a particularly suitable dispersant towards the direct exfoliation of graphite into graphene in aqueous medium.[46] Hydrophobins are surface-active microbial adhesion proteins involved in the growth and development of filamentous fungi, and are quite unique in that they exhibit a patch of hydrophobic residues on one side of their external surface (Fig. 1a), making such type of biomolecules strongly amphiphilic in nature. By contrast, many conventional proteins tend to confine the hydrophobic residues in their interior and mostly expose hydrophilic residues on their outer surface. As a matter of fact, sonication of graphite in an aqueous solution of the class II hydrophobin HFBI (obtained from the fungus *Trichoderma*

*reesei)* afforded colloidal suspensions of high quality, micrometric and submicrometric graphene platelets that were stabilized by a layer of protein molecules adsorbed through their hydrophobic patch (Fig. 1b and c). The same authors were also able to capitalize on the ample possibilities of chemical modification associated to proteins to generate graphene-based functional hybrids or composite materials, providing three specific examples in this regard.[46,47] In one of them, an HFBI dimer having the two protein domains connected by a disulfide bond was used to exfoliate and disperse graphene flakes. Subsequently, Au nanoparticles coated with mercaptosuccinic acid could be selectively anchored onto the graphene flakes by way of the disulfide bridges present in the adsorbed dimers. In another case, the HFBI protein was appended with a peptide segment (ZE, to give the fusion protein HFBI-ZE) that can specifically recognize and bind a complementary peptide (ZR) in a highly pH-sensitive manner. At a pH value of 3 (5), the ZE and ZR peptides experience electrostatic repulsion (attraction). Thus, the attachment of ZR-functionalized Au NPs onto HFBI-ZE-exfoliated graphene could be hindered or promoted at will simply by means of pH control.

In the third example, HFBI was combined with two units of a protein denoted as cellulose-binding domain (CBD) that displays a high binding affinity towards cellulose, to yield the fusion protein HFBI-DCBD (Fig. 1d).[47] Similar to the other HFBI variants, this fusion protein could exfoliate and strongly adsorb onto graphene, but at the same time it was also able to attach to nanofibrillated cellulose (NFC) through the two engineered CBD units (Fig. 1e, left picture). Such a dual binding ability facilitated the generation of high performance NFC-graphene composite films with both components being intimately mixed and interacting strongly via the fusion protein (Fig. 1e, right picture). Indeed, tensile tests revealed that the mechanical properties of the composites improved very significantly (Young´s modulus and tensile strength values increased by

a factor of 2–3 compared with the NFC-only film) at low graphene loadings (1.25 wt%). The key role played by the HFBI-DCBD stabilizer was made apparent by noting that when this fusion protein was replaced by the wild-type, HFBI-only hydrophobin, which can just bind to graphene but not to cellulose, the resulting NFC-graphene composites were inhomogeneous (Fig. 1f) and were mechanically much weaker.

More recently, another class of hydrophobins (class I) has also been tested for its ability to exfoliate and disperse graphene. Class I hydrophobins tend to possess a higher hydrophobic character than that of their class II counterparts, which drastically limits their solubility in water. Specifically, Gravagnuolo *et al* have used the class I hydrophobin Vmh2, derived from the fungus *Pleurotus ostreatus*, as a graphene dispersant in ethanol/water mixtures.[48] Since Vmh2 features much extended hydrophobic patches on its surface, it could not be used as a dispersant in water alone, but required a solvent with lower polarity instead.[49] Thus, 60 vol% ethanol in water was found to be an optimum medium for the efficient exfoliation and dispersion of graphite assisted by Vmh2, yielding high quality, few-layer graphene suspensions at significant concentrations (~0.5 mg $mL^{-1}$) that were stable for several months. Electrokinetic analysis suggested that the Vmh2-coated graphene flakes were colloidally stabilized by electrostatic repulsion stemming from a net positive charge present on the protein. Likewise, taking advantage of the fact that the aggregation state of Vmh2 can be controlled by environmental factors, solvent polarity in particular, homogeneous Vmh2-graphene hybrid films could be prepared at the air-liquid interface simply by increasing the solvent polarity (adding water to the ethanol-water mixture).

In addition to hydrophobins, other proteins have been identified as efficient graphene dispersants, in particular lysozyme (Lys) from chicken egg white[50,51] and BSA.[52,53] Indeed, graphite powder could be exfoliated and dispersed in water to give

graphene in the form of single-, few- and multi-layer flakes at concentrations up to ~0.2 mg $mL^{-1}$ using Lys.[50] This protein exhibits a strongly cationic character and consequently a high isoelectric point (pI ~10.7) due to the abundance of residues having primary amines (i.e., arginine and lysine) in its structure. As a result, the Lys-coated graphene flakes could be colloidally stabilized by electrostatic repulsion at pH below and above 10.7, but flocculated around the pI value of the protein. Furthermore, negatively charged Au NPs were successfully anchored onto the graphene flakes via the cationic Lys molecules, and the resulting hybrids were shown to possess a remarkable catalytic activity as evaluated through the reduction of *o*-nitroaniline to *o*-phenylenediamine by $NaBH_4$ as a model reaction. The catalytic activity of the Au NPs in the hybrids was seen to be much higher than that of their stand-alone counterparts, which was attributed to the enhanced stability against coalescence and aggregation when the NPs are adhered onto graphene via Lys. With a view to their use in biomedical applications, Joseph and co-workers investigated the cytotoxicity of Lys-exfoliated graphene towards a number of cell lines: mouse embryonic fibroblasts (NIH-3T3), human colorectal cancer cells (HCT-116), human cervical cancer cells (HeLa) and squamous carcinoma cells (SCC-7).[51] At a graphene concentration in the culture medium of 25 μg $mL^{-1}$ the viability of the three cancer cell lines was much lower than that of the fibroblasts, suggesting that Lys-coated graphene flakes could be used as anticancer agents. The same authors also demonstrated that calf histone was efficient at exfoliating graphene, whereas ovalbumin and bovine hemoglobin failed to afford stable graphene suspensions.

BSA has been very recently used as a particularly effective protein towards the high-throughput production of few-layer graphene flakes.[52] To this end, shear-based exfoliation in a simple kitchen blender was implemented instead of the more common

sonication treatment (Fig. 2a-c), which furnished much higher graphene production rates (up to 4-7 mg $mL^{-1}$ $h^{-1}$). The performance of BSA was compared with that of other proteins, including β-lactoglobulin (from bovine milk), ovalbumin (egg white) and hemoglobin (bovine blood), and the results suggested that the density of negative charge on the protein is central to its efficiency as a graphene dispersant. Thus, BSA possessed the highest density of negative charge at pH 7 and consequently led to the highest production rates. Another attractive feature of this protein was the fact that it afforded aqueous graphene dispersions at unusually high concentrations (up to ~7 mg $mL^{-1}$). The BSA-coated graphene dispersions were also shown to be relatively stable under biologically relevant conditions (50% fetal bovine serum), which should facilitate their use in biomedicine and bioengineering applications. In a related work, Ahadian *et al* demonstrated that BSA-stabilized graphene flakes (in this case, exfoliated via sonication) also exhibited a reasonable stability in phosphate-buffered saline (PBS) solution.[53] Furthermore, cell proliferation tests carried out with C2C12 mouse myoblasts on BSA-exfoliated graphene films revealed a similar behavior to that observed on conventional Petri dishes (Fig. 2d and e), indicating this type of graphene to be biocompatible and non-cytotoxic. The BSA-coated graphene flakes were also compounded with methacrylated gelatin to give composite hydrogels with tunable electrical conductivity and Young´s modulus, which are promising as scaffolds to, e.g., regulate the behavior of electro-active cells or the differentiation and fate of stem cells.

A number of layered TMDs have also been successfully exfoliated and/or dispersed in water using BSA.[39,54] Guan *et al* reported the production of very stable (> 1 year) and rather concentrated (> 1 mg $mL^{-1}$) aqueous suspensions of $MoS_2$, $WS_2$ and $WSe_2$ nanosheets using a cumulative layer-by-layer exfoliation route that relied on a low power bath sonication treatment for extended periods of time (48 h).[39] BSA was shown

to perform better as a TMD dispersant than synthetic polymers (polyacrylic acid, polyvinyl pyrrolidone) and other biomolecules (chitosan, gelatin). Likewise, depending on the concentration of BSA in the solution, dispersions dominated by single-layer ([BSA] < 2 mg $mL^{-1}$) or multilayer ([BSA] ~2-4 mg $mL^{-1}$) nanosheets could be attained. Owing to their very high surface area, the BSA-stabilized single-layer $MoS_2$ nanosheets demonstrated good adsorption capacity towards the pesticide 2,4-dichlorophenoxyacetic acid as well as a decent specific capacitance with aqueous 0.1 M $Na_2SO_4$ as the electrolyte. A good biocompatibility of the exfoliated $MoS_2$ nanosheets was also suggested on the basis of cell viability tests (MTT assay) carried out with fibroblasts.[39] Indeed, single-layer BSA-bound $MoS_2$ nanosheets showed a cell viability percentage that doubled that of $MoS_2$ nanosheets colloidally stabilized with surfactants, such as poly(acrylic acid) and polyvinylpyrrolidone, indicating its higher biocompatibility.

BSA-stabilized $WS_2$ nanosheets have also been used simultaneously as an efficient photothermal therapy (PTT) agent and as a photosensitizer carrier for photodynamic therapy (PDT), affording enhanced effects in the eradication of HeLa cancer cells.[54] In this case, the starting bulk $WS_2$ powder was pre-exfoliated in the absence of BSA through a grinding step followed by intercalation with $H_2SO_4$ and then ultrasonic treatment in water. The resulting pre-exfoliated $WS_2$ nanosheets were subsequently incubated with BSA to finally give BSA-stabilized $WS_2$ dispersions, which were colloidally stable in PBS medium. These nanosheets exhibited a noticeable although somewhat limited effect as PTT agent under near-infrared laser irradiation (808 nm, 1 W $cm^{-2}$, 10 min) against HeLa cells (cell viability ~50 % relative to the control sample). Likewise, the BSA-coated $WS_2$ flakes could be loaded with significant amounts of methylene blue (MB; up to 0.1 mmol $g^{-1}$), thus potentially serving as a carrier of this photosensitizer for use in PDT. However, irradiation (665 nm LED lamp, 50 mW $cm^{-2}$,

3 min) of HeLa cells incubated with the BSA-$WS_2$-MB system yielded again rather mediocre results (cell viability ~65% relative to control). A similar outcome was obtained using free MB. On the other hand, a combined PTT and PDT treatment with BSA-$WS_2$-MB, whereby irradiation using the 808 nm laser was followed by exposure to the 665 nm LED lamp, led to much improved results (cell viability < 20%). It was inferred that irradiation of the $WS_2$ nanosheets with the near-infrared laser, in addition to directly providing some PTT effect on the cancer cells, triggered the desorption of the MB molecules adsorbed on the nanosheets. In turn, the desorbed MB molecules were much more efficient as PDT agents than their adsorbed counterparts, since the generation of singlet oxygen (the main reactive species produced in PDT to induce cellular death) was not impaired by the presence of an adjacent $WS_2$ nanosheet. As a result of these synergistic PTT and PDT effects, an enhanced anti-cancer activity was obtained. Finally, due to the high atomic number of W, the authors could also use the BSA-stabilized $WS_2$ nanosheets as contrast agents for X-ray computed tomography imaging.

Ge and co-workers have employed gelatin, a mixture of proteins and peptides obtained by partial hydrolysis of collagen, towards the exfoliation and dispersion of few-layer graphene, $MoS_2$, $WS_2$ and h-BN flakes in water at reasonably high concentrations (~1 mg $mL^{-1}$).[55] Owing to its good biodegradability and biocompatibility, gelatin is potentially useful as a substrate and/or carrier in tissue engineering,[56] but its poor mechanical properties constitute a significant obstacle to such an application. In the search of a solution to this issue, the authors implemented a simple method whereby the gelatin-stabilized graphene dispersions were processed into solid gelatin-graphene composite films, with the graphene flakes acting as mechanical reinforcement of the gelatin matrix. Composite films incorporating 1 wt% graphene

boasted a 73% increase in tensile strength and 180% increase in Young´s modulus relative to the pure gelatin film. More recently, the same method has been used to prepare gelatin/h-BN composite films from gelatin-exfoliated h-BN flakes, which were then tested for oxygen barrier applications.[57] At h-BN loadings of ~2.3 wt%, the oxygen permeability of the composite decreased by a factor of 20 at a gas pressure of 1.5 bar and by a factor of 500 at 2 bar compared with the pure gelatin film in the absence of h-BN.

Although a number of proteins have demonstrated their utility as dispersants for graphene and other 2D materials, in many cases their mechanism of adsorption on (and stabilization of) such materials remains poorly understood. For hydrophobins a reasonable guess can be made, as discussed above, on account of their having large segregated domains of hydrophobic nature on their external surface, which confers them a strongly amphiphilic character. On the other hand, the situation for more conventional, water-soluble proteins, including Lys and BSA, appears to be more complicated: these proteins do not generally possess spatially segregated sequences of hydrophobic residues, as hydrophobins do, and in their native state they tend to expose hydrophilic residues to the aqueous medium and to confine hydrophobic ones in their interior so as to minimize their solvation free energy.[58] This observation suggests that proteins that can colloidally stabilize graphene and other 2D materials in water could undergo conformational changes to promote their adsorption (such changes could be further triggered by the additional energy and external forces introduced into the system during exfoliation, e.g. via sonication). Indeed, there exists some experimental evidence in support of such a hypothesis for the case of Lys- and BSA-stabilized graphene.[51,52]

Relevant insight on the issue of protein adsorption onto graphene has been recently disclosed from a theoretical perspective.[59] Although previous computational work based

on density functional theory (DFT) and molecular dynamics (MD) addressed the interaction of single amino acids with graphene in vacuum as well as under more realistic aqueous environment,[53,60-62] it has been recognized that the adsorption behavior of proteins or even peptides cannot be just extrapolated from the results obtained for their individual constituting amino acids.[62] Rather, the whole structure of the protein needs to be considered to arrive at a faithful description of its adsorption on a substrate. With this objective in mind, extensive MD simulations have been used to investigate the adsorption of bovine fibrinogen and BSA on graphene, taking the presence of water molecules from the solvent medium explicitly into account.[59] The results indicated that both proteins experienced conformational changes to make aromatic residues (e.g., tryptophan or tyrosine) originally confined in their interior interact with the graphene surface via π-π stacking. Significantly, it was also found that basic residues, such as arginine and lysine, were even more relevant than aromatic ones in driving the adsorption of the proteins onto graphene (Fig. 3a). Such *a priori* unexpected outcome was rationalized by noting that the number of water molecules in the first solvation shell around the positively charged basic residues decreased by a relatively small extent upon adsorption of the residue on graphene. Thus, the loss of electrostatic contributions to the solvation free energy of the residue was accordingly small, which could be compensated by a favorable residue-graphene van der Waals interaction. By contrast, a very recent MD simulation of BSA adsorption on graphene that used the same explicit solvent model for the water molecules suggested that BSA undergoes minimal conformational changes under free adsorption and only experiences significant changes in the presence of an external force acting on the protein.[63] Such a discrepancy between this and the previous work could be due to limitations associated to the MD theoretical approach, such as the accuracy of the different force fields employed in the simulations.[63]

The relevance of protein conformational changes has also been highlighted in a very recent study involving soy protein and graphite nanoplatelets.[64] It was observed that the ability of this protein to stabilize the platelets in water was remarkably enhanced when trifluoroethanol (TFE) was added to the suspension and the temperature was raised to 90 ºC. MD simulations revealed that such an improvement was the result of protein denaturation by the combined action of TFE and temperature, so that the hydrophobic residues originally hidden in the protein core became exposed to the surrounding medium and thus could adsorb on and colloidally stabilize the graphite platelets (Fig. 3b).

Compared with proteins, little work has been reported on the use of peptides for the direct exfoliation and colloidal stabilization of 2D materials. As a matter of fact, this issue has just been addressed for the first time in a study that compared the efficiency of 18 amphiphilic peptides and lipopeptides, both of anionic and cationic nature, towards the ultrasound-assisted exfoliation of graphite in water to give few- and multi-layer graphene flakes.[65] These peptides were structurally similar to conventional surfactants in that they were made up of a hydrophobic tail incorporating a short sequence of hydrophobic amino acid residues, plus an optional alkyl chain, and a polar ionic head containing either a protonated amine ($-NH_3^+$) or a deprotonated carboxyl ($-COO^-$) group (Fig. 4a and b). It was generally observed that the anionic peptides performed better as graphene dispersants than their cationic counterparts (Fig. 4c). The authors proposed that the establishment of cation-π interactions between cationic peptides and the polyaromatic surface of graphene would lead to a relatively low electrostatic repulsion between graphene flakes coated with such a type of peptides, and hence to a limited colloidal stability of their dispersions. The best exfoliation/dispersion results were attained with the anionic peptide $I_3C$ (IleIleIleCys) and its gemini surfactant-like dimer

$I_3C–CI_3$, which was attributed to the previously demonstrated strong ability of these peptides to self-assemble both in the bulk aqueous medium and at the water-solid interface.[66]

*2.2. Nucleotides, RNA and DNA*

Nucleotides are organic molecules consisting of three components, namely, an aromatic nitrogenous base (nucleobase) of non-polar, hydrophobic nature, a sugar moiety with five carbon atoms and a strongly polar (poly)phosphate group. This structural make-up implies that nucleotides exhibit an amphiphilic character that could be harnessed towards their use as dispersants in the direct exfoliation and stabilization of 2D materials. Similarly, nucleic acids such as RNA and DNA, which are long polymeric sequences assembled from certain sets of nucleotides as monomers, constitute *a priori* good candidates for the same purpose. However, in spite of their strong potential, work on the use of nucleotides and nucleic acids as dispersants for the direct exfoliation of 2D materials has been limited.

To this day, only one nucleotide [flavin mononucleotide (FMN), a derivative of vitamin $B_2$] has been used for the exfoliation/dispersion of graphite,[67–69] its performance being outstanding in several respects. The chemical structure of FMN incorporates a dimethylated isoalloxazine unit as the nucleobase, a ribitol moiety and a single phosphate group (Fig. 5a). FMN had been previously used as a surfactant for carbon nanotubes[70] and it was known from theoretical calculations that the adsorption energy of its isoalloxazine unit on the nanotube wall is high.[71] Likewise, prior circumstantial evidence in a different context had revealed that FMN adsorbs strongly onto reduced graphene oxide nanosheets,[72] suggesting that it could also make an efficient dispersant in the preparation of oxide- and defect-free graphene flakes. This hypothesis was

substantiated later on when pristine graphite powder could be successfully exfoliated and dispersed in aqueous FMN solutions via sonication (Fig. 5b and c).[67] Significantly, graphene suspensions with long-term stability could be attained using a very low amount of FMN relative to graphene (FMN/graphene mass ratios as low as ~0.04). This result was in marked contrast with what is usually reported in the preparation of surfactant-stabilized graphene, where surfactant/graphene ratios one or two orders of magnitude larger are the norm.[36,73–75] Having a very low fraction of dispersant is generally desirable because its presence can be detrimental to the performance of materials and devices obtained thereof.[16] For instance, films assembled from graphene flakes stabilized with a low amount of FMN exhibited remarkable electrical conductivity (~52000 S $m^{-1}$) without the need to resort to post-treatments (e.g., high temperature annealing). Furthermore, the use of FMN as a dispersant led to highly concentrated graphene suspensions (up to ~50 mg $mL^{-1}$; see inset to Fig. 5c), again outperforming most efficient surfactants previously used for the same purpose.

FMN has also exhibited a notable templating ability towards the unzipping of graphene flakes into graphene nanoribbons. This was demonstrated by Yoon *et al*,[68] who exfoliated graphite flakes in aqueous FMN solution using a cup-horn sonicator. After discarding most of the resulting dispersion through sedimentation at a high centrifugal force (80000 *g*), a nanoribbon-enriched supernatant was obtained (Fig. 5d). The nanoribbons were ~10-100 nm wide and ~250 nm long on average, and could not be obtained using other dispersants such as sodium dodecyl sulfate or sodium cholate. Detailed studies by transmission electron microscopy led the authors to propose that the adsorption of linear assemblies of FMN molecules onto exfoliated graphene flakes triggered the unzipping of the flakes into nanoribbons via sonication (inset to Fig. 5d). The linear self-assembly of FMN onto graphene was driven by two specific features of

the isoalloxazine moiety: (i) its strong binding affinity towards graphitic surfaces and (ii) its propensity to form hydrogen bonds with neighboring isoalloxazine moieties.

Most work on the direct exfoliation of graphite to give colloidally dispersed graphene relies on ultrasound or shear forces to cleave the graphite layers. However, the latter approaches are not without their limitations, including a low exfoliation yield (usually <5 wt%).[16] To address this issue, researchers have combined electrochemical pre-exfoliation of graphite with ultrasound-/shear-assisted liquid-phase dispersion of the pre-exfoliated material.[76] Depending on the specific experimental conditions, electrochemical exfoliation can lead to very high quality and thin (1-3 monolayers) graphene flakes, which could be advantageous application-wise.[77,78] FMN has been recently employed as a dispersant for different graphite types that had been pre-exfoliated by an electrochemical (anodic) method in aqueous $K_2SO_4$ solution.[69] In all cases, the amount of FMN-stabilized graphene produced was much larger than that obtained when only sonication or shear forces were used. Thin films of the electrochemically exfoliated, FMN-stabilized graphene flakes demonstrated good biocompatibility towards the murine fibroblast cell line L-929, suggesting their prospective utility in biomedicine.[69]

The growth of metal or semiconducting nanoparticles (NPs) on pristine graphene to form functional hybrids is frequently troublesome due to the absence of strong anchoring sites in the graphene support. In the case of FMN-exfoliated graphene this problem could be overcome, and defect-free flakes incorporating large numbers of noble metal (Ag, Pt and Pd) NPs with sizes in the 3–25 nm range were readily prepared.[67] The ionic phosphate group in FMN molecules adsorbed on the graphene flakes was thought to facilitate the nucleation of the NPs from their metallic precursors. The resulting metal NP-graphene hybrids were tested as catalysts for the reduction of

nitroarenes, exhibiting activities comparable or even higher than those of the best performing metal catalysts previously investigated. The hybrids were also evaluated as electrocatalysts towards the oxygen reduction reaction with a view to their use as electrochemical oxygen sensors (Fig. 5e). A linear range of response to oxygen concentration from 0.30 to 7.6 mg $L^{-1}$ was observed (inset to Fig. 5e), with limits of detection between 0.25 and 0.29 mg $L^{-1}$.

It has been known for more than a decade that nucleic acids (DNA and RNA in particular) are able to debundle and disperse individual CNTs in aqueous medium. [44,79] In the case of DNA, a previous denaturation step was often required to cleave the double-stranded biomolecule (dsDNA) into single-stranded DNA (ssDNA), so that a strong ssDNA-CNT interaction can be established through π-π stacking between the nucleobases and the nanotube sidewall. As previously noted, it was also suggested that nucleic acids are able to wrap around CNTs in a helical fashion, giving rise to well-stabilized colloidal systems. [44] However, such a helical conformation is not expected to be in place in the stabilization of 2D materials. This was probably one of the reasons why early efforts on the direct exfoliation of graphite assisted by ssDNA relied on the covalent incorporation of a pyrene moiety at one end of the nucleic acid strand, so that the strong pyrene-graphene interaction would facilitate the immobilization of the biomolecule on the 2D structure.[80] Nevertheless, subsequent studies demonstrated that nucleic acids are able to exfoliate and colloidally stabilize both graphene[81,82] and other 2D materials ($WS_2$ and $WSe_2$; Fig. 6a and b)[83] by themselves, i.e. without the assistance of attached moieties. Furthermore, dsDNA could be directly employed towards the exfoliation of graphite into graphene via sonication[82]: it was postulated that the large amount of energy introduced into the system during sonication sufficed to disrupt the hydrogen bonding in the dsDNA molecule, thus yielding individual ssDNA strands and

circumventing the need of a prior denaturation step. In all cases, stable aqueous suspensions of single- and few-layer flakes with lateral sizes in the ~0.1-1 μm range and significant concentrations (up to ~2 mg $mL^{-1}$) were attained, denoting the effectiveness of nucleic acids as dispersants of 2D materials.

First-principles calculations based on DFT revealed that all the nucleobases present in DNA and RNA, i.e. adenine (A), thymine (T), guanine (G), cytosine (C) and uracil (U), physisorbed on the surface of graphene, $MoS_2$ and $WS_2$ with relatively high binding energies in the ~65-90 kJ $mol^{-1}$ range and following the order G > A > T > C > U.[84] MD simulations have also been carried out to investigate the dispersion of graphene flakes by short ssDNA segments (3-18 nucleobases) in aqueous medium.[85,86] Both homologous (i.e., containing only one type of nucleobase) and mixed (AGTC repetition) base sequences were considered. In general, the results indicated that the investigated oligonucleotides are efficient graphene dispersants. However, their dispersing ability was seen to depend on the specific base sequence and was dictated by the interplay of three competing interactions: (i) π-π stacking between nucleobases within the ssDNA molecule, (ii) hydrogen bonding between ssDNA and water molecules, and (iii) nucleobase-graphene π-π stacking.[85] For the homologous oligonucleotides, the strength of their adsorption onto graphene was governed by the nature of the repeating nucleobase, as it followed the same trend as that obtained for the single (monomeric) nucleosides in aqueous medium. Nevertheless, the oligonucleotide with the mixed base sequence was predicted to be the best dispersant on account of its higher propensity to lie flat on the graphene surface in an elongated conformation, which maximized the number of nucleobases interacting with the latter.

Concerning the practical use of nucleic acid-exfoliated 2D materials, a number of possibilities have been explored. For example, thin films made from RNA-exfoliated

graphene flakes have demonstrated a performance as transparent conductors that is comparable to that of graphene films obtained using synthetic surfactants.[81] Likewise, graphene-Au nanoparticle hybrids with potential utility in sensing or catalysis have been prepared through specific binding of ssDNA-stabilized graphene flakes to Au NPs labeled with complementary ssDNA strands.[80] In the biomedical realm, ssDNA-exfoliated $WS_2$ and $WSe_2$ flakes have been very recently investigated for their antibacterial effect.[83] It was determined that the viability of *Escherichia coli* cells decreases markedly upon exposure to aqueous dispersions of these TMD flakes at a concentration of 80 μg $mL^{-1}$ (Fig. 6c). Best results were obtained for ssDNA-exfoliated $WSe_2$, affording a decrease in viability of ~80 %, whereas a more modest performance (~40-50 %) was attained with $WS_2$ and graphene oxide, the latter also studied for comparison purposes. Control experiments suggested that bacterial damage was probably caused by direct oxidation of cellular components through contact with the 2D sheets without the generation of reactive oxygen species. In a different work, graphene exfoliated with dsDNA as a dispersant has been shown to inhibit the migration of cancer cells in zebrafish embryos (human tumor xenograft model) to an extent similar to that achieved using the commercially available anticancer drug paclitaxel (Fig. 6d).[82] Because tumor-free embryos appeared to be viable following exposure to the graphene flakes, the results indicated that this material might be used as a drug to prevent cancer metastasis.

### *2.3. Polysaccharides and plant extracts*

Polysaccharides are polymeric carbohydrate molecules composed of long chains of monosaccharide units bound together by glycosidic linkages. Cellulose is the most abundant polysaccharide; in fact, it is the most profuse organic biopolymer on Earth. It

consists of a linear chain of several hundreds to many thousands of D–glucose units linked by β(1→4) glycosidic bonds. The amphiphilicity of cellulose comes from the presence of both hydrophilic hydroxyl groups in equatorial positions on the glucopyranose rings and of hydrophobic C–H moieties in axial positions,[87] and manifests itself, e.g., by the formation of emulsions in water–oil mixtures.[88] Cellulose has been shown to be useful as an amphiphilic exfoliating agent and dispersant of graphene and other 2D materials. Indeed, Carrasco *et al* obtained stable, concentrated aqueous dispersion of mostly single–layer graphene by direct liquid–phase exfoliation of graphite using a low relative amount of cellulose nanocrystals.[89] In this case, the colloidal stabilization was aided by the presence of abundant sulfate groups in the nanocrystals coming from their extraction process with sulfuric acid.

Another form of cellulose that has found use as amphiphilic dispersant for graphene and other 2D materials is microfibrillated or nanofibrillated cellulose (NFC). NCF is a mesoscopic material with a length in the micrometer scale and diameters of just a few nanometers that constitutes an important structural reinforcing component of the primary cell wall of green plants. It can be obtained, usually as a hydrogel, by mechanical disintegration of macroscopic pulp fibers. Its excellent mechanical properties make NCF attractive as filler for nanocomposites with improved mechanical properties. However, its propensity to aggregate poses an important obstacle for such application. Malho and co–workers circumvented this problem by first directly exfoliating and dispersing graphite in NFC hydrogel to yield homogeneous aqueous dispersions of multi–layered graphene flakes and then preparing nanocomposites by removal of water through filtration.[90] No aggregation of the NFC fraction occurred during the process. Instead, the resulting nanocomposites consisted of linear co-assemblies of graphene layers and NFC, and displayed a superior combination of

stiffness, toughness and strength. Hydrophobic and aromatic ring polarization interactions of the graphene surface with the pyranose rings of cellulose were assumed to be the driving force for the co–assembly between graphene and NFC as well as the origin of the enhanced mechanical properties of the composite. Such interactions have been previously reported to arise between the aromatic residues of proteins and cellulose,[91–93] thus supporting the idea that a similar interaction mechanism might apply in the graphene-cellulose case. We have previously mentioned that the fusion protein HFBI–DCBD was used to mediate the binding between NFC and graphene, and thus to strengthen the resulting composite material.[47] Indeed, this protein–mediated binding was more efficient than that of the present nanocomposite consisting of just NFC and graphene in that it led to a higher stiffness; nevertheless, the composite also exhibited a lower flexibility and toughness. NFC is also an efficient dispersant for other 2D materials, such as h–BN and $MoS_2$.[88] Strong and flexible NFC-exfoliated $MoS_2$ films were successfully used as Na–ion battery anodes for prospective flexible battery applications. Parenthetically, levulinic acid (4–oxopentanoic acid), which is derived from the degradation of cellulose, has been very recently put forward as an environmentally friendly, biomass–derived solvent (rather than dispersant) for the scalable production of defect-free single–layered graphene from graphite.[94] Specifically, it was claimed that flakes less than 1.0 nm in thickness, taken as single–layered graphene, were found to comprise ~84% of the total dispersed flakes.

Lignin is the second most abundant natural polymer after cellulose and the most abundant aromatic renewable material on the planet. It is a key structural material in the supporting tissues of vascular plants, forming cell walls in wood and bark, to which it lends rigidity and hydrophobicity. Lignin is a cross–linked polymer consisting of three types of phenylpropane subunits connected in complex ways (see Fig. 7a). Although it

is predominantly hydrophobic, it also contains weakly acidic groups, namely, phenolic and carboxylic groups that are negatively charged in alkaline condition. Different lignin derivatives are obtained depending on the particular process used for its extraction, namely, the kraft pulping process produces alkali lignin (AL), while the sulfite pulping process produces sodium lignosulfonate (SL). Both processes lead to an increase in hydrophilicity via the introduction of new phenolic groups through the kraft pulping process[95] and sulfonate groups through the sulfite process. The amphiphilic polyelectrolyte SL was previously shown to be an excellent dispersant for CNTs,[96] and very recently Lou and co-workers have demonstrated its efficiency in the case of graphene.[97] Indeed, the latter were able to obtain stable aqueous graphene dispersions at unusually high concentrations (up to 13.5 mg $mL^{-1}$). In addition, Liu *et al* have demonstrated AL–assisted exfoliation of a variety of lamellar materials (graphite, $MoS_2$, $WS_2$, and h–BN) in aqueous media.[98,99] The graphene flakes prepared with AL were tested as mechanical reinforcement filler for epoxy resin matrixes, proving them to be more efficient than commercial nano–additives such as CNTs or carbon nanofibers. The presence of graphene flakes at a loading of 0.1 wt% rendered the fractured surface of the epoxy/graphene composite (Fig. 7b and c) rougher than that of the neat epoxy resin (not shown), hampering crack propagation (Fig. 7c) and thus increasing the required strain for fracture.[98] $MoS_2$ flakes exfoliated with AL were tested as a cathode for Li-ion batteries, displaying a reversible capacity of 164 mA h $g^{-1}$ (Fig. 7d), which remained above 110 mA h $g^{-1}$ at 12 C (Fig. 7e), and excellent rate capabilities compared to its bulk counterpart.[99] Such an enhanced performance was partly rationalized by the ultrathin nature of the exfoliated $MoS_2$ flakes, which greatly increases the surface area available for contact with the electrolyte and in turn shortens the electron and ion

migration lengths. On the other hand, the relatively small lateral size of the flakes increased the fraction of edge sulfur atoms that were assumed to act as redox centers.

Gum Arabic (GA), or gum acacia, is the best known of the tree gum exudates and can be obtained easily and abundantly. GA is a low–cost, environmentally friendly edible emulsifier with a high solubility in water over a broad pH range, and is extensively used in the processing of drugs, foods and drinks. Its structure comprises both hydrophilic hyperbranched polysaccharides (mainly galactose and arabinose) and hydrophobic glycoproteins. Stable ink dispersions of CNTs prepared by sonication of CNT bundles in aqueous GA solution had been previously reported,[100] suggesting that GA could also be an effective stabilizer in the case of graphene. This possibility was indeed demonstrated by both Guardia *et al*[35] and Chabot and co-workers.[101] The latter showed that GA adsorbed onto the graphene flakes could be totally removed by filtration and acid hydrolysis to yield pure multilayer graphene powder with a yield of 5 wt%. Fan *et al* used GA–stabilized graphene dispersions to prepare Ag–graphene hybrids, which were found to be suitable substrates for the detection of 4–aminothiophenol by surface–enhanced Raman spectroscopy in liquid environment.[102] Graphene dispersed with glycidyl methacrylate–modified GA could be introduced into a poly(acrylic acid) hydrogel at a loading of 5 wt%, significantly improving its mechanical properties.[103]

Chitosan (CS) is a naturally occurring linear cationic polysaccharide composed of randomly distributed β-(1-4)-linked D-glucosamine and N-acetyl-D-glucosamine units. It is extracted via deacetylation of chitin from shrimp and other crustacean shells by treatment with NaOH. CS comprises both hydrophobic, non–polar acetyl chain segments and hydrophilic, positively charged amino groups. Owing to its biodegradability, biocompatibility, antimicrobial activity and excellent film–forming

ability, CS has drawn interest in such diverse fields as pharmaceutics, fuel cells, agriculture or food science.[104] CS has been reported to promote the dispersibility of CNTs in aqueous medium.[105-107] More recently, Unalan and co–workers have described the CS-assisted exfoliation of graphite using short (30 min) sonication times, affording 5.5 mg $mL^{-1}$ aqueous dispersions of high quality graphene flakes.[108] As for $MoS_2$, Feng *et al* reported its exfoliation and dispersion in acidic aqueous CS solution to prepare CS-$MoS_2$ composites with good dispersion of the 2D filler, leading to a material with improved structural stability as well as mechanical and thermal properties.[109] It has also been found that well-dispersed, CS-exfoliated $MoS_2$ flakes increased the flame retardance and reduced the smoke toxicity of $MoS_2$-epoxy resin composites.[110] Such improvements were tentatively explained on the basis of a barrier effect provided by the ultrathin $MoS_2$ flakes. Restriction of both external heat and oxygen flow would explain the improved flame retardance, while inhibition of the escape of volatile toxic substances would reduce the smoke toxicity.

Single–layer $MoS_2$ flakes have been recently put forward as a novel near–infrared (NIR) absorbing agent, exhibiting higher absorbance in the NIR region than, e.g., gold nanorods.[111] Using CS-exfoliated $MoS_2$ aqueous dispersions, the spectroscopic properties of $MoS_2$ have been combined with the ability of CS to impart physiological stability and biocompatibility towards the development of phototherapy systems against cancer in two instances in the literature (Fig. 8). In the first example (Fig. 8a and b), Yin *et al* developed a chemotherapeutic drug nanocarrier for a NIR light-triggered drug delivery system.[112] To this end, $MoS_2$ flakes with controllable size were obtained through an exfoliation process based on oleum treatment (Fig. 8a, step 1) and stabilized in aqueous solution with the assistance of CS (Fig. 8a, step 2). Doxorubicin (DOX), a common chemotherapeutic drug, could be loaded onto the CS-modified $MoS_2$ flakes

(Fig. 8a, step 3) without detriment to the colloidal stability of the dispersion. Then, NIR light-induced local hyperthermia acted as a stimulus for the on–off control of DOX release from the CS–modified $MoS_2$ flakes (Fig. 8b). In the second example (Fig. 8c), Zhang and co-workers used an ionic liquid-assisted grinding method in the presence of CS to obtain CS-modified $MoS_2$ flakes, which performed satisfactorily towards *in vitro* PTT tests with human hepatocyte carcinoma (HepG2) cells.[113] These biocompatible and colloidally stable CS–modified $MoS_2$ flakes were also used as a contrast agent in X–ray computed tomography imaging due to the ability of Mo to absorb X–rays.[112]

A variety of other polysaccharides, including hyaluronic acid (HA),[114] pullulan,[108] guar gum[115] and xantham gum,[115] have been identified as exfoliating and/or dispersing agents for graphite and other layered materials. HA is an anionic polysaccharide (specifically, a glycosaminoglycan) that constitutes an essential component of the extracellular matrix of connective, epithelial and neural tissues. Pyrene has been appended to HA molecules to introduce the possibility of π–π stacking with graphitic systems, and the resulting amphiphilic biopolymer has been found to facilitate the aqueous exfoliation not only of graphite but also of h–BN and $MoS_2$.[114] Culinary hydrocolloids such as guar gum, xantham gum and tannic acid (a polyphenol) have facilitated the exfoliation and dispersion of $MoS_2$ in water, which could be subsequently decorated with Au nanoparticles via *in situ* reduction by the hydrocolloids. The resulting hybrids exhibited an excellent catalytic activity in the reduction of 4–nitrophenol with $NaBH_4$.[115] Finally, several medicinal plant extracts have also been tested as mediators for the direct exfoliation of graphite, although with mixed results. The most successful were extracts from cocklebur (*Xanthium strumarium*) and Japanese mugwort (*Artemisia princeps*).[116] In these cases, stable aqueous dispersions of multilayer graphene flakes could be obtained with a reported yield of ~6 wt%.

*2.4. Bile salts*

Bile acids are a type of steroid acids present in many vertebrates and primarily synthesized by the liver from cholesterol. Their main biological function is to act as natural surfactants for the emulsification of lipids, facilitating digestion of the latter by the organism.[117] The amphiphilic character of bile acids (or their salt forms) is provided by a core made up of four non-aromatic rings (three cyclohexane rings and one cyclopentane ring) appended with an alkyl chain that is terminated by a polar carboxylic or sulfonic acid group [e.g., see Fig. 9a (left) for the structure of sodium cholate (SC)]. The planar four-ring section possesses a number (typically 2 or 3) of hydroxyl groups located on one side of the molecule, making this face hydrophilic in nature while the opposite face remains hydrophobic [see Fig. 9a (right) for the case of SC]. As demonstrated by MD simulations,[118,119] this configuration favors the adsorption of the bile salt onto graphene and CNT surfaces (and probably other hydrophobic nanostructures), with its hydrophobic face contacting the graphitic surface (even though π-π stacking will not be in place) and its hydrophilic face exposed to the aqueous environment, thereby promoting the role of the bile salt as a dispersant for such nanostructures. Indeed, the potential of bile salts as dispersants for the colloidal stabilization of carbon nanostructures was first disclosed by Wenseleers *et al*, who demonstrated their remarkable ability to exfoliate and disperse CNT bundles into individual entities.[120]

The use of bile salts in the colloidal preparation of 2D materials was pioneered by the groups of Hersam[121] and Coleman.[122,123] The latter have subsequently devoted considerable research efforts with this type of dispersant to address several key issues towards the implementation of wet direct exfoliation as a competitive production

method. In this endeavor, the bile salt (SC in most cases) was mainly employed as a benchmark surfactant due to its convenience as regards processing and characterization purposes. For example, SC is a readily available and rather innocuous compound that is transparent to visible as well as near and middle ultraviolet light. In early work with bile salts, SC-water solutions were combined with long sonication times to demonstrate that aqueous graphene and TMD suspensions can be procured at significant concentrations (~0.5 mg $mL^{-1}$).[123,124] By contrast, initial reports using other surfactants and shorter sonication could only exfoliate graphene at very low concentrations (<0.05 mg $mL^{-1}$),[125] which are impractical for many applications. More recently, SC was employed as an aqueous dispersant to introduce and implement the concept of shear exfoliation of graphite and other layered solids to give few-layer flakes of the corresponding 2D material.[126] The main advantage of this method compared with sonication-induced exfoliation lies in the fact that under conditions relevant for scale-up (i.e., for large production volumes) both the rate and yield of production of the 2D materials are much higher (~1-2 orders of magnitude).

Colloidal dispersions of 2D materials obtained by the direct exfoliation methods considered here are typically polydisperse in nature, implying that as-prepared samples generally comprise a mixture of flakes with different lateral sizes (length, L) and thicknesses (number of monolayers, N).[127] To determine these morphological parameters, researchers have relied on microscopy techniques (e.g., transmission electron and/or atomic force microscopy) to measure L and N for a statistically significant number of individual flakes transferred from the liquid phase to a proper substrate. However, this process can be extremely time-consuming, so the availability of a fast *in situ* diagnosis tool would be most desirable. In this regard, it has been noted that the optical extinction spectra of several 2D materials ($MoS_2$, $WS_2$, graphene)

contain quantitative information about the mean L and N values for the flakes in the dispersion.[127–129] This question was first investigated in the case of $MoS_2$, using SC as a dispersant due to its optical transparency in the relevant wavelength range.[127] To this end, Backes *et al* prepared a set of aqueous $MoS_2$ dispersions with different lateral size and thickness distributions by sorting a stock SC-stabilized suspension via a straightforward centrifugation approach referred to as band sedimentation (Fig. 9b). As noticed from Fig. 9c, some features in the extinction spectra were strongly dependent on the specific sorted fraction. More to the point, the ratio of extinction at the B-exciton peak located at ~605 nm and the local minimum at ~345 nm ($Ext_B/Ext_{345}$) was directly correlated with the mean flake length in the dispersion (Fig. 9d). This result could be rationalized by taking into account that the local electronic structure, and hence the local optical properties and spectral shape, of the flake edges differs from that of the inner region of the flakes. Because the relative fraction of edge regions increases as the lateral size of the flake decreases, the shape of the optical spectrum will be size-dependent, so that a quantitative relationship between L and $Ext_B/Ext_{345}$ could be derived. Likewise, the position of the A-exciton peak ($\lambda_A$, ~660-675 nm range) was seen to be dependent on N owing to quantum confinement effects (Fig. 9e), so that an empiric formula relating $\lambda_A$ and N was obtained. More recently, similar quantitative spectroscopic metrics have also been established for both $WS_2$[128] and graphene[129] using the same or similar methodological approaches. Considering that optical extinction spectroscopy is a readily available technique in most laboratories worldwide, these results can be expected to expedite the development of liquid-phase exfoliated 2D materials towards many uses.

Although post-production processing based on centrifugation can be implemented to sort the originally polydisperse colloidal suspensions of 2D materials into samples

with narrow lateral size and/or thickness distributions,[121,127–129] such processes tend to be tedious and time-consuming. A way to circumvent any post-processing steps in the size selection of liquid-phase exfoliated $MoS_2$ has been recently proposed by Varrla *et al*.[130] The authors demonstrated that flakes with mean length and thickness between ~40 and 200 nm and ~2 and 12 monolayers, respectively, can be controllably tuned simply by adjusting the concentration of SC used during the exfoliation step (smaller and thinner flakes are obtained at higher SC concentrations). This finding is important because it provides a convenient access to $MoS_2$ flakes with sizes that can be optimized towards specific target applications (see below). At present, only SC has been shown to possess a capability for flake size selection during exfoliation, the origin of which is not well understood. As a tentative explanation, it has been argued that size selection arises from differences in packing density of SC molecules between edge and basal plane regions of $MoS_2$ due to electronic structure and geometrical effects.[130]

In addition to SC, other bile salts have been tested as dispersants for graphene, including sodium deoxycholate (SDOC), sodium taurodeoxycholate (STDOC) and 3-[(3-cholamidopropyl)dimethyl ammonio]-1-propanesulfonate (CHAPS).[35,131,132] Like SC, SDOC and STDOC are anionic dispersants, implying that they provide stability to colloidal systems via electrostatic repulsion, whereas CHAPS possesses a zwitterionic character. The main advantage of some of these bile salts as compared with the case of SC lies chiefly in their ability to afford aqueous graphene suspensions at significantly higher concentrations (up to ~12 mg $mL^{-1}$ with STDOC),[131,132] which can be advantageous when considering practical applications (e.g., for the development of graphene-based conductive inks).

Bile salt-exfoliated 2D materials (graphene and $MoS_2$ in particular) have shown potential towards different prospective applications in, e.g., catalysis, energy storage or

biosensing. In the case of graphene, these include its use as transparent and conducting films[121,122] and support of Pt NPs for the oxygen reduction reaction.[131] For $MoS_2$, thin films of this TMD blended with an electrically conductive nanostructured carbon material (SC-dispersed graphene or CNTs) were tested as thermoelectric devices and cathodes for Li-ion batteries.[123] Significantly, the electrical conductivity of the films ($\sigma$) could be increased by several orders of magnitude upon addition of the nanostructured carbon, while their Seebeck coefficient (S) only decreased to a limited extent. As a result, the power factor of $MoS_2$/CNT hybrid films ($P = S^2\sigma$), a measure of the utility of a material as a thermoelectric device, reached remarkable values ($P = 87\ \mu W\ K^{-2}\ m^{-1}$ for a film with 75 wt% CNT loading). As a cathode for Li-ion batteries, the SC-exfoliated $MoS_2$-CNT hybrid films exhibited a good capacity retention (>70%) and high coulombic efficiency (>95%) after 100 charge-discharge cycles. Furthermore, the ability to control the lateral dimensions of liquid-exfoliated $MoS_2$ flakes (either by post-production centrifugation or through specific concentrations of SC) has been shown to be beneficial in catalytic applications, for instance when $MoS_2$ is used as an electrocatalyst for the hydrogen evolution reaction (HER).[127,130] Taking into account that the catalytically active sites of $MoS_2$ are mostly located at the flake edges,[133] the performance of this 2D material towards the HER should be improved as the mean lateral size of the flakes in the tested sample is decreased. Indeed, larger current densities and lower onset potentials associated to better HER response were measured from $MoS_2$ flakes prepared via exfoliation at higher SC concentrations, which yielded smaller mean flake sizes (Fig. 9f).[130] Very recently, a systematic comparison of the HER activity of thin films of different SC-exfoliated TMDs ($MoS_2$, $MoSe_2$, $MoTe_2$, $WS_2$, $WSe_2$, $WTe_2$) has been carried out.[134] The activity was found to be in the order selenides > sulfides > tellurides, with $MoSe_2$ as the best-performing electrocatalyst. The

exact origin of these differences in catalytic performance is currently unknown. One possibility would be a higher intrinsic activity of the catalytic sites in the selenides, which were assumed to be located at the flake edges (like in the case of $MoS_2$). Alternatively, the density of catalytically active sites could be higher for the selenides, for example due to a lower propensity to become deactivated via functionalization with impurities during exfoliation. In any case, the catalytic activity of all the tested TMDs could be significantly improved by increasing the film thickness (larger number of active sites) and by adding carbon nanotubes to the film (higher electrical conductivity of the electrode).

The colloidal stability of charge-stabilized dispersions is known to sensitively depend on a number of parameters, including the concentration of electrolytes.[135] Capitalizing on these effects, Li *et al* have recently developed a label-free colorimetric DNA biosensor based on a SC-exfoliated (and therefore charge-stabilized) aqueous $MoS_2$ suspension.[136] It was observed that the as-prepared suspension ($MoS_2$ concentration: 0.05 mg $mL^{-1}$) became destabilized and sedimented when an electrolyte (NaCl, $10^{-2}$ M) was added. However, salt-induced sedimentation could be inhibited in the presence of ssDNA oligonucleotides (7.5 nM). This effect was ascribed to co-adsorption of ssDNA on $MoS_2$, with its negatively charged phosphate groups providing the flakes with enhanced resistance to charge screening by the electrolyte and hence with improved colloidal stability. On the other hand, when the complementary ssDNA oligonucleotide was included in the mixture, hybridization between the two complementary strands to give dsDNA took place, which involved desorption of the ssDNA strands from $MoS_2$ and consequently sedimentation of the latter. Under such conditions, the extent of sedimentation (or equivalently, the amount of $MoS_2$ remaining in dispersion) was seen to depend on the concentration of the complementary ssDNA in

the mixture. Thus, a straightforward method to quantitatively detect this ssDNA could be put in place by measuring the optical extinction of the remaining $MoS_2$ dispersion at a given wavelength (672 nm). A linear range of measurement between 0.5 and 7.5 nM with a detection limit of 0.3 nM was determined. This approach was also sensitive enough to detect polymorphisms in the ssDNA strands at the single-nucleotide level.

*2.5. Other bio-related compounds*

Besides the different classes of biomolecules discussed in the preceding subsections, a number of other bio-related compounds have been explored towards the exfoliation and dispersion of 2D materials (mostly graphene). A rather atypical example in this regard is that of saccharin. Although saccharin is indeed an artificial organic compound, it is nonetheless non-toxic, biocompatible and widely used in the food industry as a sweetener. This compound has been recently employed as both intercalating and dispersing agent towards the electrochemical (anodic) exfoliation of graphite in aqueous medium.[137] Phospholipids, a type of naturally occurring molecules that make up the basic scaffold of cell membranes, constitute another example. Such compounds are amphiphilic substances comprised of two long alkyl chains connected by a polar head that incorporates a phosphate group, and are known to strongly interact with graphitic surfaces.[138] It has been experimentally demonstrated that lecithin, a phospholipid mixture extracted from, e.g., soybeans or egg yolk, can be used to exfoliate and disperse graphite into few-layer, defect-free graphene at modest concentrations (~0.05 mg $mL^{-1}$) in chloroform.[139] MD simulations suggested that stabilization was achieved through adsorption of reverse micelles and hemimicelles on the graphitic basal plane, where a large number of alkyl chains were directly exposed to the solvent medium and provided a steric barrier to flake coagulation. Phospholipid (liposome)-exfoliated graphene has also been prepared both in water and PBS medium

at concentrations of ~0.1-0.2 mg $mL^{-1}$ and successfully tested as an efficient antibacterial agent.[140] Specifically, moderate concentrations (0.05 mg $mL^{-1}$) of these graphene flakes were found to inhibit bacterial growth for both Gram-positive (*Staphylococcus aureus*) and Gram-negative *(Escherichia coli*) strains in a way comparable to that achieved with graphene oxide (growth reduction of ~85-90% relative to an isotonic saline solution taken as control sample). The extent of growth reduction was significantly smaller when the bacterial strains were exposed to phospholipids in the absence of graphene flakes, highlighting the relevant role played by the 2D carbon material as an antibacterial agent.

Urea, an environmentally friendly organic compound generated as a by-product of the metabolism of nitrogen-containing substances in mammals, has also been recently employed for the exfoliation of graphite[141] and h-BN[142] to give few-layer flakes in aqueous suspension. We note, however, that urea is not an amphiphilic compound, so that the mechanisms involved in its ability to colloidally disperse these materials deserve special attention. In the case of graphene, which was exfoliated through probe sonication, experimental evidence suggested that the ultrasonic treatment triggered the reaction between the primary amine group of urea molecules adsorbed on graphene and $CO_2$ dissolved in the aqueous medium from air.[141] Such a reaction furnished the urea molecule with a –NHCOOH group that can subsequently deprotonate and provide colloidal stability to the graphene flakes via electrostatic repulsion. Regarding h-BN, exfoliation was accomplished by means of a solid-state ball milling process in the presence of urea (typical h-BN:urea mass ratios of 1:60; see Fig. 10a).[142] Significantly, the as-milled product could be directly dispersed in water at a high yield (85 wt%) without the need of sonication. The dispersions were comprised of 1–2 nm thick, amino-functionalized h-BN flakes with a small lateral size (~50–100 nm; Fig. 10b) and

could be prepared at concentrations up to ~30 mg $mL^{-1}$ (Fig. 10c, left photograph). It was proposed that mechano-chemical processes during ball milling facilitated both exfoliation of the bulk h-BN particles and functionalization of the resulting thin flakes at edges and defects with urea-derived amine groups. Furthermore, gelling of the highly concentrated suspensions was observed when left undisturbed for two weeks (Fig. 10c, right photograph), which afforded extremely lightweight h-BN aerogels (densities down to ~1.4 mg $cm^{-3}$) after a freeze-drying step (Fig. 10d). Thin, transparent films were also produced through vacuum filtration of the aqueous h-BN dispersions, which exhibited strong ultraviolet and blue light emission that could be useful in bioimaging, lasing or optoelectronic applications.

Drug molecules have also been used towards the exfoliation and dispersion of graphene in aqueous medium. For example, ball milling of graphite with the antifungal drug amphotericin B was shown to afford water-dispersible, few-layer graphene flakes, even though this compound is hydrophobic in nature and therefore possesses very low water solubility.[143] The mechanism behind the ability of amphotericin B to stabilize graphene in water was not investigated and is currently unknown, although the molecule was assumed to be adsorbed on the exfoliated flakes. However, pharmacological and biocompatibility tests indicated that this graphene was essentially inactive against many fungi species of the *Candida* genus (the free drug is highly toxic to fungi) and lacked significant toxicity to human lung epithelial cells (A549 line). The biological inertness of amphotericin B-loaded graphene towards fungi was attributed to the fact that the drug cannot reach the site of action at the fungus cell membrane at therapeutic concentrations when it is strongly bound to graphene. On the other hand, chlorin e6, an efficient photosensitizer drug in PDT, has been used as a dispersant for graphene in aqueous medium (Fig. 10e and f).[144] Like amphotericin B, this drug molecule exhibits a poor

solubility in water, but in this case the colloidal stabilization mechanism was known from previous studies with CNTs:[145] adsorption of chlorin e6 on the graphene surface through π-π interaction yielded a charge-transfer complex that induced a strong polarity in this molecule, which in turn afforded aqueous dispersibility to the graphene-chlorin e6 hybrid system. Furthermore, the graphene-chlorin e6 hybrid was used as a PDT agent towards the destruction of HeLa cancer cells. Specifically, the viability of HeLa cells exposed to concentrations of chlorin e6 loaded onto graphene of 0.05, 0.10 and 0.20 μg $mL^{-1}$ decreased dramatically (down to ~4%) upon irradiation with 660 nm laser light, whereas no significant effect was observed when free chlorin e6 was employed instead (Fig. 10g). Such concentrations of the photosensitizer were much smaller than those required when chlorin e6 was combined with carriers other than pristine graphene (e.g., graphene oxide[146] or conjugated polymers).[147] The experiments revealed that the graphene-chlorin e6 complex was internalized by the HeLa cells much more efficiently than free chlorin e6. Once in the cytosol, part of the photosensitizer molecules desorbed from the graphene flakes and were able to induce the generation of reactive oxygen species through absorption of the 660 nm light, which in turn triggered cell death. Because graphene itself also absorbs 660 nm light and heats up as a result, some contribution to cellular death by a PTT mechanism was thought to be in place as well.

## 3. Summary and outlook

Significant research efforts carried out over the last few years have laid the foundations for the use of biomolecules as exfoliating and dispersing agents towards the production of 2D materials from their bulk layered counterparts. This biomolecule-based approach typically exploits the amphiphilicity of many bio-related compounds to afford flakes of the 2D materials in aqueous medium, which is advantageous for

environmental, safety and other practical reasons. A relatively wide variety of biomolecules, such as proteins and peptides, nucleotides and nucleic acids, polysaccharides or bile salts, have already demonstrated their utility in this regard, so that the basic library of biodispersants of 2D materials has now been established. We expect this library to expand in the future with the addition of further compounds from the different classes of biomolecules that have been identified. Table 1 provides a summary list with the specific bio-related compounds that have been used to this day as dispersants for 2D materials, as well as information on the particular exfoliation methods used, the typical concentrations attained for the resulting colloidal suspensions and some applications tested with these biomolecule-exfoliated materials. The performance of some small biomolecules, such as certain amphiphilic peptides, sodium cholate or flavin mononucleotide, is comparable to or even better than that of many synthetic surfactants of similar molecular weight reported before. It also becomes immediately apparent that most work in this research area has focused on graphene, although progress with TMDs and h-BN has also been substantial. However, there is no reason to believe that the production of other classes of 2D materials (particularly those that also exhibit some degree of hydrophobicity) cannot benefit from the use of biomolecules as exfoliating and/or dispersing agents.

As discussed in the previous sections and similar to the case of synthetic surfactants, the colloidal stabilization of 2D materials in the aqueous phase by biomolecules is based on adsorption of the latter onto the surface of the flakes, which in turn generally relies on relatively weak (non-covalent) interactions such as van der Waals forces or π-π stacking. This weak interaction has its own advantages and drawbacks. For instance, the atomic and electronic structure, and therefore many of the attractive properties of the pristine 2D material, is largely preserved in the biomolecule-

exfoliated flakes.[48,52,67,123,126,141] On the other hand, the biomolecule-stabilized flakes could experience competitive adsorption when exposed to media that incorporate certain (natural or synthetic) compounds. This effect could either serve a good purpose (e.g., it can be used to load drugs on the flakes with a view to biomedical applications or to adsorb pollutants from wastewater for environmental remediation)[39,54] or have negative consequences; for example, it could lead to coagulation of the originally stable colloidal dispersions. When competitive adsorption is to be avoided, the use of biomolecules that have demonstrated a particularly strong binding affinity to the 2D material, such as hydrophobins[46,47] or flavin mononucleotide[67] in the case of graphene, would be preferred.

It is apparent that biomolecule-exfoliated 2D materials are particularly promising platforms for a range of applications in the biomedical field. However, such applications will not come to fruition unless the long-term effects on living organisms as well as the distribution pattern in organs/tissues and fate of such materials are thoroughly evaluated and understood. At present, this type of information is mainly lacking for 2D materials in general and their biomolecule-exfoliated counterparts in particular. Instead, most biocompatibility tests reported in the literature for, e.g., protein-exfoliated graphene or $MoS_2$ flakes have been limited in scope and have focused on short-term (a few days) tests.[39,53] Connected with this question is the issue of potential conformational change associated to the use of certain large biomolecules, especially proteins, as exfoliating and/or dispersing agents. For example, there is indication that some proteins undergo denaturation when they are employed as stabilizers in the sonication-induced exfoliation of graphite into graphene.[51,52] At present, it is unknown on a protein-by-protein basis whether denaturation is just the result of direct protein-graphene interactions or is triggered by the external stimuli applied to the system (i.e., ultrasound), but in either

case it can have negative effects (e.g., loss of a desired function of the protein or emergence of unwanted interactions in biological media). There are, however, some possible strategies that could be implemented to preserve the native state of the protein upon its adsorption onto the 2D material. For example, it has been shown that the carbohydrate-binding protein Concanavalin A retains its biological activity upon adsorption onto CVD-grown graphene films if the graphene-protein interface is appropriately engineered (specifically, using a multivalent, pyrene-based tripodal molecule as protein anchor).[148] By contrast, loss of function was observed when the protein was directly adsorbed onto the graphene film. A similar approach could be used for the preparation of aqueous dispersions of graphene flakes. To avoid the possible deleterious effect of ultrasound treatment on the protein conformation, exfoliation by shear mixing could be a reasonable option: it has been demonstrated that shear rates at least as high as $2\times10^5$ $s^{-1}$ are not able to denature globular proteins in water.[149] We note that these shear rates are typically employed for the exfoliation of layered materials.[126]

The rich chemistry associated to many large biomolecules, including nucleic acids and proteins, provides ample opportunities to further tune the interfacial characteristics and functionality of the exfoliated 2D materials towards different practical applications, for example, to attain a highly selective and specific recognition of biological and other targets or to modulate the colloidal dispersibility of the flakes. Nevertheless, with a few exceptions,[46,47,150] this possibility has remained largely untapped. In this regard, functional nucleic acids such as aptamers and nucleic acid enzymes (ribozymes, deoxyribozymes) can be designed and synthesized *à la carte* to have a high binding affinity and selectivity towards specific targets.[151] These nucleic acids could be used as multifunctional systems, affording simultaneously the exfoliation and/or dispersion of the 2D material and the selective recognition of molecular species, so that the as-

prepared nucleic acid-stabilized flakes could be directly used in, e.g., biosensing or medical diagnosis applications. It is worth mentioning that many biosensors based on the combination of graphene with functional nucleic acids have been previously reported in the literature,[152] but these prior efforts did not typically incorporate the role of the biomolecule as a dispersant in the production of graphene itself.

Overall, this review has shown that significant advances in the production of 2D materials by direct liquid-phase exfoliation methods as well as in the implementation of such materials towards practical applications can be made possible by the use of biomolecules as exfoliating/dispersing agents. We believe that this research area will further benefit from the many possibilities for development that lie ahead as regards the incorporation of biomolecules in both the mentioned and additional functional roles.

**Acknowledgments**

Financial support from the Spanish MINECO and the European Regional Development Fund (ERDF) through project MAT2015-69844-R as well as from "Plan de Ciencia, Tecnología e Innovación 2013-2017 del Principado de Asturias" and ERDF (project GRUPIN14-056) is gratefully acknowledged.

**References**

1. M. Xu, T. Liang, M. Shi and H. Chen, *Chem. Rev.*, 2013, **113**, 3766-3798.

2. A. C. Ferrari, F. Bonaccorso, V. I. Fal'ko, K. S. Novoselov, S. Roche, P. Bøggild, S. Borini, F. Koppens, V. Palermo, N. Pugno, J. A. Garrido, R. Sordan, A. Bianco, L. Ballerini, M. Prato, E. Lidorikis, J. Kivioja, C. Marinelli, T. Ryhänen, A. Morpurgo, J. N. Coleman, V. Nicolosi, L. Colombo, A. Fert, M. Garcia-Hernandez, A. Bachtold, G. F. Schneider, F. Guinea, C. Dekker, M. Barbone, C. Galiotis, A. Grigorenko, G.

Konstantatos, A. Kis, M. Katsnelson, C. W. J. Beenakker, L. Vandersypen, A. Loiseau, V. Morandi, D. Neumaier, E. Treossi, V. Pellegrini, M. Polini, A. Tredicucci, G. M. Williams, B. H. Hong, J. H. Ahn, J. M. Kim, H. Zirath, B. J. van Wees, H. van der Zant, L. Occhipinti, A. Di Matteo, I. A. Kinloch, T. Seyller, E. Quesnel, X. Feng, K. Teo, N. Rupesinghe, P. Hakonen, S. R. T. Neil, Q. Tannock, T. Löfwander and J. Kinaret, *Nanoscale*, 2015, **7**, 4598–4810.

3. H. Zhang, *ACS Nano*, 2015, **10**, 9451-9469.

4. V. Nicolosi, M. Chhowalla, M.G. Kanatzidis, M.S. Strano and J.N. Coleman, *Science*, 2013, **340**, 1226419.

5. G. Fiori, F. Bonaccorso, G. Iannaccone, T. Palacios, D. Neumaier, A. Seabaugh, S.K. Banerjee and L. Colombo, *Nat. Nanotechnol.*, 2014, **9**, 768-779.

6. F. Xia, H. Wang, D. Xiao, M. Dubey and A. Ramasubramaniam, *Nat. Photon.*, 2014, **8**, 899-907.

7. H. Wang, H. Feng and J. Li, *Small*, 2014, **10**, 2165-2181.

8. H.Y. Mao, S. Laurent, W. Chen, O. Akhavan, M. Imani, A.A. Ashkarran and M. Mahmoudi, *Chem. Rev.*, 2013, **113**, 3407-3424.

9. Y. Chen, C. Tan, H. Zhang and L. Wang, *Chem. Soc. Rev.*, 2015, **44**, 2681-2701.

10. Y. Liu, X. Dong and P. Chen, *Chem. Soc. Rev.*, 2012, **41**, 2283-2307.

11. P.K. Kannan, D.J. Late, H. Morgan and C.S. Rout, *Nanoscale*, 2015, **7**, 13293-13312.

12. X. Fan, G. Zhang and F. Zhang, *Chem. Soc. Rev.*, 2015, **44**, 3023-3035.

13. F. Bonaccorso, A. Lombardo, T. Hasan, Z. Sun, L. Colombo and A.C. Ferrari, *Mater. Today*, 2012, **15**, 564-589.

14. Y. Zhang, L. Zhang and C. Zhou, *Acc. Chem. Res.*, 2013, **46**, 2329-2339.

15. Y. Shi, H. Li and L.-J. Li, *Chem. Soc. Rev.*, 2015, **44**, 2744-2756.

16. L. Niu, J.N. Coleman, H. Zhang, H. Shin, M. Chhowalla and Z. Zheng, *Small*, 2016, **12**, 272-293.

17. A. Ciesielski and P. Samorì, *Chem. Soc. Rev.*, 2014, **43**, 381-398.

18. A. Ciesielski and P. Samorì, *Adv. Mater.*, 2016, DOI: 10.1002/adma.201505371.

19. D.R. Dreyer, S. Park, C.W. Bielawski and R.S. Ruoff, *Chem. Soc. Rev.*, 2010, **39**, 228-240.

20. D. Chen, H. Feng and J. Li, *Chem. Rev.*, 2012, **112**, 6027-6053.

21. M. Chhowalla, H.K. Shin, G. Eda, L.-J. Li, K.P. Loh and H. Zhang, *Nat. Chem.*, 2013, **5**, 263-275.

22. D. Voiry, A. Mohite and M. Chhowalla, *Chem. Soc. Rev.*, 2015, **44**, 2702–2712.

23. E. Morales-Narváez and A. Merkoçi, *Adv. Mater.*, 2012, **24**, 3298-3308.

24. S. Navalon, A. Dhakshinamoorthy, M. Alvaro and H. Garcia, *Chem. Rev.*, 2014, **114**, 6179-6212.

25. M.A. Lukowski, A.S. Daniel, F. Meng, A. Forticaux, L. Li and S. Jin, *J. Am. Chem. Soc.*, 2013, **135**, 10274-10277.

26. M.A. Lukowski, A.S. Daniel, C.R. English, F. Meng, A. Forticaux, R.J. Hamers and S. Jin, *Energy Environ. Sci.*, 2014, **7**, 2608-2613.

27. L. Guardia, J.I. Paredes, J.M. Munuera, S. Villar-Rodil, M. Ayán-Varela, A. Martínez-Alonso and J.M.D. Tascón, *ACS Appl. Mater. Interfaces*, 2014, **6**, 21702-21710.

28. M. Acerce, D. Voiry and M. Chhowalla, *Nat. Nanotechnol.*, 2015, **10**, 313-318.

29. R. Rozada, J.I. Paredes, M.J. López, S. Villar-Rodil, I. Cabria, J.A. Alonso, A. Martínez-Alonso and J.M.D. Tascón, *Nanoscale*, 2015, **7**, 2374-2390.

30. Y. Hernandez, V. Nicolosi, M. Lotya, F. M. Blighe, Z. Y. Sun, S. De, I. T. McGovern, B. Holland, M. Byrne, Y. K. Gun'ko, J. J. Boland, P. Niraj, G. Duesberg, S. Krishnamurthy, R. Goodhue, J. Hutchison, V. Scardaci, A. C. Ferrari and J. N. Coleman, *Nat. Nanotechnol.*, 2008, **3**, 563–568.

31. Y. Hernandez, M. Lotya, D. Rickard, S.D. Bergin and J.N. Coleman, *Langmuir*, 2010, **26**, 3208-3213.

32. J. N. Coleman, M. Lotya, A. O'Neill, S. D. Bergin, P. J. King, U. Khan, K. Young, A. Gaucher, S. De, R. J. Smith, I. V. Shvets, S. K. Arora, G. Stanton, H. Y. Kim, K. Lee, G. T. Kim, G. S. Duesberg, T. Hallam, J. J. Boland, J. J. Wang, J. F. Donegan, J. C. Grunlan, G. Moriarty, A. Shmeliov, R. J. Nicholls, J. M. Perkins, E. M. Grieveson, K. Theuwissen, D. W. McComb, P. D. Nellist and V. Nicolosi, *Science*, 2011, **331**, 568–571.

33. S. Ravula, S.N. Baker, G. Kamath and G.A. Baker, *Nanoscale*, 2015, **7**, 4338-4353.

34. R.J. Smith, M. Lotya and J.N. Coleman, *New J. Phys.*, 2010, **12**, 125008.

35. L. Guardia, M.J. Fernández-Merino, J.I. Paredes, P. Solís-Fernández, S. Villar-Rodil, A. Martínez-Alonso and J.M.D. Tascón, *Carbon*, 2011, **49**, 1653-1662.

36. J.-W.T. Seo, A.A. Green, A.L. Antaris and M.C. Hersam, *J. Phys. Chem. Lett.*, 2011, **2**, 1004-1008.

37. L. Guardia, J.I. Paredes, R. Rozada, S. Villar-Rodil, A. Martínez-Alonso and J.M.D. Tascón, *RSC Adv.*, 2014, **4**, 14115-14127.

38. N.D. Mansukhani, L.M. Guiney, P.J. Kim, Y. Zhao, D. Alducin, A. Ponce, E. Larios, M.J. Yacaman and M.C. Hersam, *Small*, 2016, **12**, 294–300.

39 G. Guan, S. Zhang, S. Liu, Y. Cai, M. Low, C.P. Teng, I.Y. Phang, Y. Cheng, K.L. Duei, B.M. Srinivasan, Y. Zheng, Y.-W. Zhang and M.-Y. Han, *J. Am. Chem. Soc.*, 2015, **137**, 6152-6155.

40. H.-J. Butt, K. Graf and M. Kappl, *Physics and Chemistry of Interfaces*, Wiley-VCH, Weinheim, 2003, ch. 12.

41. V. Zorbas, A. Ortiz-Acevedo, A.B. Dalton, M.M. Yoshida, G.R. Dieckmann, R.K. Draper, R.H. Baughman, M. Jose-Yacaman and I.H. Musselman, *J. Am. Chem. Soc.*, 2004, **126**, 7222-7227.

42. S.S. Karajanagi, H. Yang, P. Asuri, E. Sellitto, J.S. Dordick and R.S. Kane, *Langmuir*, 2006, **22**, 1392-1395.

43. D. Nepal and K.E. Geckeler, *Small*, 2007, **3**, 1259-1265.

44. M. Zheng, A. Jagota, E.D. Semke, B.A. Diner, R.S. McLean, S.R. Lustig, R.E. Richardson and N.G. Tassi, *Nat. Mater.*, 2003, **2**, 338-342.

45. A.B. Bourlinos, V. Georgakilas, R. Zboril, T.A. Steriotis, A.K. Stubos and C. Trapalis, *Solid State Commun.*, 2009, **149**, 2172-2176.

46. P. Laaksonen, M. Kainlauri, T. Laaksonen, A. Shchepetov, H. Jiang, J. Ahopelto and M.B. Linder, *Angew. Chem. Int. Ed.*, 2010, **49**, 4946-4949.

47. P. Laaksonen, A. Walther, J.-M. Malho, M. Kainlauri, O. Ikkala and M.B. Linder, *Angew. Chem. Int. Ed.*, 2011, **50**, 8688-8691.

48. A.M. Gravagnuolo, E. Morales-Narváez, S. Longobardi, E.T. da Silva, P. Giardina and A. Merkoçi, *Adv. Funct. Mater.*, 2015, **25**, 2771-2779.

49. S. Longobardi, D. Picone, C. Ercole, R. Spadaccini, L. De Stefano, I. Rea and P. Giardina, *Biomacromolecules*, 2012, **13**, 743-750.

50. K. Qu, L. Wu, J. Ren and X. Qu, *Nano Res.*, 2013, **6**, 693-702.

51. D. Joseph, N. Tyagi, A. Ghimire and K.E. Geckeler, *RSC Adv.*, 2014, **4**, 4085-4093.

52. A. Pattammattel and C.V. Kumar, *Adv. Funct. Mater.*, 2015, **25**, 7088-7098.

53. S. Ahadian, M. Estili, V.J. Surya, J. Ramón-Azcón, X. Liang, H. Shiku, M. Ramalingam, T. Matsue, Y. Sakka, H. Bae, K. Nakajima, Y. Kawazoe and A. Khademhosseini, *Nanoscale*, 2015, **7**, 6436-6443.

54. Y. Yong, L. Zhou, Z. Gu, L. Yan, G. Tian, X. Zheng, X. Liu, X. Zhang, J. Shi, W. Cong, W. Yin and Y. Zhao, *Nanoscale*, 2014, **6**, 10394-10403.

55. Y. Ge, J. Wang, Z. Shi and J. Yin, *J. Mater. Chem.*, 2012, **22**, 17619-17624.

56. M. Santoro, A.M. Tatara and A.G. Mikos, *J. Control. Release*, 2014, **190**, 210-218.

57. J. Biscarat, M. Bechelany, C. Pochat-Bohatier and P. Miele, *Nanoscale*, 2015, **7**, 613-618.

58. J.F. Zayas, *Functionality of Proteins in Food*, Springer-Verlag, Berlin, 1997, ch. 1.

59. Z. Gu, Z. Yang, L. Wang, H. Zhou, C.A. Jimenez-Cruz and R. Zhou, *Sci. Rep.*, 2015, **5**, 10873.

60. N. Dragneva, W.B. Floriano, D. Stauffer, R.C. Mawhinney, G. Fanchini and O. Rubel, *J. Chem. Phys.*, 2013, **139**, 174711.

61. Z.E. Hughes, S.M. Tomásio and T.R. Walsh, *Nanoscale*, 2014, **6**, 5438-5448.

62. Z.E. Hughes and T.R. Walsh, *J. Mater. Chem. B*, 2015, **3**, 3211-3221.

63. J.G. Vilhena, P. Rubio-Pereda, P. Vellosillo, P.A. Serena and R. Pérez, *Langmuir*, 2016, **32**, 1742-1755.

64. Y. Jewel, T. Liu, A. Eyler, W.-H. Zhong and J. Liu, *J. Phys. Chem. C*, 2015, **119**, 26760-26767.

65. M. Cao, N. Wang, L. Wang, Y. Zhang, Y. Chen, Z, Xie, Z. Li, E. Pambou, R. Li, C. Chen, F. Pan, H. Xu, J. Penny, J.R.P. Webster and J.R. Lu, *J. Mater. Chem. B*, 2016, **4**, 152-161.

66. M. Cao, C. Cao, P. Zhou, N. Wang, D. Wang, J. Wang, D. Xia and H. Xu, *Colloid Surf. A-Physicochem. Eng. Asp.*, 2015, **469**, 263-270.

67. M. Ayán-Varela, J.I. Paredes, L. Guardia, S. Villar-Rodil, J.M. Munuera, M. Díaz-González, C. Fernández-Sánchez, A. Martínez-Alonso and J.M.D. Tascón, *ACS Appl. Mater. Interfaces*, 2015, **7**, 10293-10307.

68. W. Yoon, Y. Lee, H. Jang, M. Jang, J.S. Kim, H.S. Lee, S. Im, D.W. Boo, J. Park and S.-Y. Ju, *Carbon*, 2015, **81**, 629-638.

69. J.M. Munuera, J.I. Paredes, S. Villar-Rodil, M. Ayán-Varela, A. Pagán, S.D. Aznar-Cervantes, J.L. Cenis, A. Martínez-Alonso and J.M.D. Tascón, *Carbon*, 2015, **94**, 729-739.

70. S.-Y. Ju, J. Doll, I. Sharma and F. Papadimitrakopoulos, *Nat. Nanotechnol.*, 2008, **3**, 356-362.

71. C.S. Lin, R.Q. Zhang, T.A. Niehaus and T. Frauenheim, *J. Phys. Chem. C*, 2007, **111**, 4069-4073.

72. M.J. Fernández-Merino, S. Villar-Rodil, J.I. Paredes, P. Solís-Fernández, L. Guardia, R. García, A. Martínez-Alonso and J.M.D. Tascón, *Carbon*, 2013, **63**, 30-44.

73. S.M. Notley, *Langmuir*, 2012, **28**, 14110-14113.

74. D. Parvez, S. Das, H.S.T. Ahmed, F. Irin, S. Bhattacharia and M.J. Green, *ACS Nano*, 2012, **6**, 8857-8867.

75. L. Zhang, Z. Zhang, C. He, L. Dai, J. Liu and L. Wang, *ACS Nano*, 2014, **8**, 6663-6670.

76. A.M. Abdelkader, A.J. Cooper, R.A.W. Dryfe and I.A. Kinloch, *Nanoscale*, 2015, **7**, 6944-6956.

77. S. Yang, M.R. Lohe, K. Müllen and X. Feng, *Adv. Mater.*, 2016, DOI: 10.1002/adma.201505326.

78. J.M. Munuera, J.I. Paredes, S. Villar-Rodil, M. Ayán-Varela, A. Martínez-Alonso and J.M.D. Tascón, *Nanoscale*, 2016, **8**, 2982-2998.

79. S. Badaire, C. Zakri, M. Maugey, A. Derré, J.N. Barisci, G. Wallace and P. Poulin, *Adv. Mater.*, 2005, **17**, 1673-1676.

80. F. Liu, J.Y. Choi and T.S. Seo, *Chem. Commun.*, 2010, **46**, 2844-2846.

81. F. Sharifi, R. Bauld, M.S. Ahmed and G. Fanchini, *Small*, 2012, **8**, 699-706.

82. D. Joseph, S. Seo, D.R. Williams and K.E. Geckeler, *ACS Appl. Mater. Interfaces*, 2014, **6**, 3347-3356.

83. G.S. Bang, S. Cho, N. Son, G.W. Shim, B.-K. Cho and S.-Y. Choi, *ACS Appl. Mater. Interfaces*, 2016, **8**, 1943-1950.

84. H. Vovusha and B. Sanyal, *RSC Adv.*, 2015, **5**, 67427-67434.

85. A.K. Manna and S.K. Pati, *J. Mater. Chem. B*, 2013, **1**, 91-100.

86. L.-J. Liang, T. Wu, Y. Kang and Q. Wang, *ChemPhysChem*, 2013, **14**, 1626-1632.

87. L.-S. Johansson, T. Tammelin, J. M. Campbell, H. Setälä and M. Österberg, *Soft Matter*, 2011, **7**, 10917-10924.

88. Y. Li, H. Zhua, F. Shen, J. Wan, S. Lacey, Z. Fang, H. Dai and L. Hu, *Nano Energy*, 2015, **13**, 346–354.

89. P. M. Carrasco, S. Montes, I. García, M. Borghei, H. Jiang, I. Odriozola, G. Cabañero and V. Ruiz, *Carbon*, 2014, **70**, 157-163.

90. J.-M. Malho, P. Laaksonen, A. Walther, O. Ikkala and M. B. Linder, *Biomacromolecules*, 2012, **13**, 1093-1099.

91. J. Lehtio, J. Sugiyama, M. Gustavsson, L. Fransson, M. Linder and T. T. Teeri, *Proc. Natl. Acad. Sci. U.S.A.*, 2003, **100**, 484-489.

92. N. K. Vyas, *Curr. Opin. Struct. Biol.*, 1991, **1**, 732-740.

93. C. Divne, J. Ståhlberg, T. T. Teeri and T. A. Jones, *J. Mol. Biol.*, 1998, **275**, 309-325.

94. M. Sharma, D. Mondal, N. Singh and K. Prasad, Chem. Commun., 2016, DOI: 10.1039/C6CC00256K.

95. W. Zhu, Ph.D. Thesis, *Equilibrium of Lignin Precipitation. The Effects of pH, Temperature, Ion Strength and Wood Origins*, Chalmers University of Technology, Gothenburg, Sweden, 2013.

96. Y. Liu, L. Gao and J. Sun, *J. Phys. Chem. C*, 2007, **111**, 1223-1229.

97. H. Lou, D. Zhu, L. Yuan, X. Qiu, X. Lin, D. Yang and Y. Li, *J. Phys. Chem. C*, 2015, **119**, 23221-23230.

98. W. Liu, R. Zhou, D. Zhou, G. Ding, J. M. Soah, C. Y. Yue and X. Lu, *Carbon*, 2015, **83**, 188-197.

99. W. Liu, C. Zhao, R. Zhou, D. Zhou, Z. Liu and X. Lu, *Nanoscale*, 2015, **7**, 9919-9926.

100. R. Bandyopadhyaya, E. Nativ-Roth, O. Regev and R. Yerushalmi-Rozen, *Nano Lett.*, 2002, **2**, 25-28.

101. V. Chabot, B. Kim, B. Sloper, C. Tzoganakis and A. Yu, *Sci. Rep.*, 2013, **3**, 1378.

102. J. Fan, Z. Shi Y. Ge, J. Wang, Y, Wang and J. Yin, *J. Mater. Chem.*, 2012, **22**, 13764-13772.

103. J. Fan, Z. Shi, J. Wang and J. Yin, *Polymer*, 2013, **54**, 3921-3930.

104. M. Rinaudo, *Prog. Polym. Sci.*, 2006, **31**, 603-632.

105. Takahashi, T. Luculescu, C. R. Uchida, K. Ishii and T. Yajima, *Chem. Lett.*, 2005, **34**, 1516-1517.

106. L. Y. Yan, Y. F. Poon, M. B. Chan-Park, Y. Chen and Q. Zhang, *J. Phys. Chem. C*, 2008, **112**, 7579-7587.

107. C. Iamsamai, S. Hannongbua, U. Ruktanonchai, A. Soottitantawat and S. T. Dubas, *Carbon*, 2010, **48**, 25-30.

108. I. U. Unalan, C. Wan, S. Trabattoni, L. Piergiovannia and S. Farris, *RSC Adv.*, 2015, **5**, 26482-26490.

109. X. Feng, X. Wang, W. Xing, K. Zhou, Lei Song and Y. Hu, *Compos. Sci. Technol.*, 2014, **93**, 76-82.

110. D. Wang, L. Song, K. Zhou, X. Yu, Y. Hu and J. Wang, *J. Mater. Chem. A*, 2015, **3**, 14307-14317.

111. S. S. Chou, B. Kaehr, J. Kim, B. M. Foley, M. De, P. E. Hopkins, J. Huang, C. J. Brinker and V. P. Dravid, *Angew. Chem. Int. Ed.*, 2013, **52**, 4160-4164.

112. W. Yin, L. Yan, J. Yu, G. Tian, L. Zhou, X. Zheng, X. Zhang, Y. Yong, J. Li, Z. Gu and Y. Zhao, *ACS Nano*, 2014, **8**, 6922-6933.

113. W. Zhang, Y. Wang, D. Zhang, S. Yu, W. Zhu, J. Wang, F. Zheng, S. Wang and J. Wang, *Nanoscale*, 2015, **7**, 10210-10217.

114. F. Zhang, X. Chen, R. A. Boulos, F. M. Yasin, H. Lu, C. Raston and H. Zhang, *Chem. Commun.*, 2013, **49**, 4845-4847.

115. S. Ravula, J. B. Essner and G. A. Baker, *ChemNanoMat*, 2015, **1**, 167-177.

116. B. K. Salunke and B. S. Kim, *RSC Adv.*, 2016, **6**, 17158-17162.

117. B. Borgström, *Acta Med. Scand.*, 1974, **196**, 1-10.

118. S. Lin, C.-J. Shih, M.S. Strano and D. Blankschtein, *J. Am. Chem. Soc.*, 2011, **133**, 12810-12823.

119. C.-J. Shih, S. Lin, M.S. Strano and D. Blankschtein, *J. Phys. Chem. C*, 2015, **119**, 1047-1060.

120. W. Wenseleers, I.I. Vlasov, E. Goovaerts, E.D. Obraztsova, A.S. Lobach and A. Bouwen, *Adv. Funct. Mater.*, 2004, **14**, 1105-1112.

121. A.A. Green and M.C. Hersam, *Nano Lett.*, 2009, **9**, 4031-4036.

122. S. De, P.J. King, M. Lotya, A. O´Neill, E.M. Doherty, Y. Hernandez, G.S. Duesberg and J.N. Coleman, *Small*, 2010, **6**, 458-464.

123. R.J. Smith, P.J. King, M. Lotya, C. Wirtz, U. Khan, S. De, A. O´Neill, G.S. Duesberg, J.C. Grunlan, G. Moriarty, J. Chen, J. Wang, A.I. Minett, V. Nicolosi and J.N. Coleman, *Adv. Mater.*, 2011, **23**, 3944-3948.

124. M. Lotya, P.J. King, U. Khan, S. De and J.N. Coleman, *ACS Nano*, 2010, **4**, 3155-3162.

125. M. Lotya, Y. Hernandez, P.J. King, R.J. Smith, V. Nicolosi, L.S. Karlsson, F.M. Blighe, S. De, Z.M. Wang, I.T. McGovern, G.S. Duesberg and J.N. Coleman, *J. Am. Chem. Soc.*, 2009, **131**, 3611-3620.

126. K. R. Paton, E. Varrla, C. Backes, R. J. Smith, U. Khan, A. O'Neill, C. Boland, M. Lotya, O. M. Istrate, P. King, T. Higgins, S. Barwich, P. May, P. Puczkarski, I. Ahmed,

M. Moebius, H. Pettersson, E. Long, J. Coelho, S. E. O'Brien, E. K. McGuire, B. Mendoza Sanchez, G. S. Duesberg, N. McEvoy, T. J. Pennycook, C. Downing, A. Crossley, V. Nicolosi and J. N. Coleman, *Nat. Mater.*, 2014, **13**, 624–630.

127. C. Backes, R.J. Smith, N. McEvoy, N.C. Berner, D. McCloskey, H.C. Nerl, A. O´Neill, P.J. King, T. Higgins, D. Hanlon, N. Scheuschner, J. Maultzsch, L. Houben, G.S. Duesberg, J.F. Donegan, V. Nicolosi and J.N. Coleman, *Nat. Commun.*, 2014, **5**, 4576.

128. C. Backes, B.M. Szydłowska, A. Harvey, S. Yuan, V. Vega-Mayoral, B.R. Davies, P. Zhao, D. Hanlon, E.J.G. Santos, M.I. Katsnelson, W.J. Blau, C. Gadermaier and J.N. Coleman, *ACS Nano*, 2016, **10**, 1589-1601.

129. C. Backes, K.R. Paton, D. Hanlon, S. Yuan, M.I. Katsnelson, J. Houston, R.J. Smith, D. McCloskey, J.F. Donegan and J.N. Coleman, *Nanoscale*, 2016, **8**, 4311-4323.

130. E. Varrla, C. Backes, K.R. Paton, A. Harvey, Z. Gholamvand, J. McCauley and J.N. Coleman, *Chem. Mater.*, 2015, **27**, 1129-1139.

131. Z. Sun, J. Masa, Z. Liu, W. Schuhmann and M. Muhler, *Chem. Eur. J.*, 2012, **18**, 6972-6978.

132. P. Ramalingam, S.T. Pusuluri, S. Periasamy, R. Veerabahu and J. Kulandaivel, *RSC Adv.*, 2013, **3**, 2369-2378.

133. T. F. Jaramillo, K. P. Jorgensen, J. Bonde, J. H. Nielsen, S. Horch and I. Chorkendorff, *Science* 2007, **317**, 100−102.

134. Z. Gholamvand, D. McAteer, C. Backes, N. McEvoy, A. Harvey, N.C. Berner, D. Hanlon, C. Bradley, I. Godwin, A. Rovetta, M.E.G. Lyons, G.S. Duesberg and J.N. Coleman, *Nanoscale*, 2016, **8**, 5737-5749.

135. D.H. Everett, *Basic Principles of Colloid Science*, Royal Society of Chemistry, London, 1988.

136. B.L. Li, H.L. Zou, L. Lu, Y. Yang, J.L. Lei, H.Q. Luo and N.B. Li, *Adv. Funct. Mater.*, 2015, **25**, 3541-3450.

137. M.K.P. Kumar, S. Shanthini and C. Srivastava, *RSC Adv.*, 2015, **5**, 53865-53869.

138. B. Luan, T. Huynh and R. Zhou, *Nanoscale*, 2016, **8**, 5750-5754.

139. M. Pykal, K. Šafářová, K.M. Šišková, P. Jurečka, A.B. Bourlinos, R. Zbořil and M. Otyepka, *J. Phys. Chem. C*, 2013, **117**, 11800-11803.

140. R. Zappacosta, M. Di Giulio, V. Ettorre, D. Bosco, C. Hadad, G. Siani, S. Di Bartolomeo, A. Cataldi, L. Cellini and A. Fontana, *J. Mater. Chem. B*, 2015, **3**, 6520-6527.

141. P. He, C. Zhou, S. Tian, J. Sun, S. Yang, G. Ding, X. Xie and M. Jiang, *Chem. Commun.*, 2015, **51**, 4651-4654.

142. W. Lei, V.N. Mochalin, D. Liu, S. Qin, Y. Gogotsi and Y. Chen, *Nat. Commun.*, 2015, **6**, 8849.

143. N. Rubio, R. Serra-Maia, H. Kafa, K.-C. Mei, K.T. Al-Jamal, W. Luckhurst, M. Zloh, F. Festy, J.P. Richardson, J.R. Naglik, E. Pach and B. Ballesteros, *Langmuir*, 2014, **30**, 14999-15008.

144. G. Liu, H. Qin, T. Amano, T. Murakami and N. Komatsu, *ACS Appl. Mater. Interfaces*, 2015, **7**, 23402-23406.

145. A. F. M. Mustafizur Rahman, F. Wang, K. Matsuda, T. Kimura and N. Komatsu. : *Chem. Sci.*, 2011, **2**, 862–867.

146. B. Tian, C. Wang, S. Zhang, L. Feng and Z. Liu. *ACS Nano* 2011, **5**, 7000−7009.

147. H. Gong, L. Cheng, J. Xiang, H. Xu, L. Feng, X. Shi and Z.Liu, *Adv. Funct. Mater.* 2013, **23**, 6059−6067.

148. T. Alava, J.A. Mann, C. Théodore, J.J. Benitez, W.R. Dichtel, J.M. Parpia and H.G. Craighead, *Anal. Chem.*, 2013, **85**, 2754-2759.

149. J. Jaspe and S.J. Hagen, *Biophys. J.*, 2006, **91**, 3415-3424.

150. D. Oh, X. Dang, H. Yi, M.A. Allen, K. Xu, Y.J. Lee and A.M. Belcher, *Small*, 2012, **8**, 1006-1011.

151. J. Liu, Z. Cao and Y. Lu, *Chem. Rev.*, 2009, **109**, 1948-1998.

152. L. Tang, Y. Wang and J. Li, *Chem. Soc. Rev.*, 2015, **44**, 6954-6980.

**Table 1.** Summary of the different biomolecules that have been reported in the literature to exfoliate and colloidally disperse graphene and other 2D materials by direct methods. Typical concentrations (conc.) of the resulting dispersions as well as explored applications for the materials derived thereof are also indicated.

| Biomolecule | 2D material | Exfoliation method | Conc. (mg $mL^{-1}$) | Applications | Refs. |
|---|---|---|---|---|---|
| *Proteins, peptides* | | | | | |
| HFBI (class II hydrophobin) | Graphene | Bath/tip sonication | 0.04 | Mechanical reinforcement of polymer composites | 46,47 |
| Vmh2 (class I hydrophobin) | Graphene | Tip sonication | 0.5 | -- | 48 |
| Bovine serum albumin | Graphene, $MoS_2$ $WS_2$, $WSe_2$ | Bath/tip sonication; shear mixing; $H_2SO_4$ intercalation | 0.2-7 | Filler of biomedical hydrogels; adsorbent for toxic compounds; supercapacitor electrode; PTT agent; carrier in PDT; CT contrast agent | 39,45,52–54 |
| Lysozyme | Graphene | Tip sonication | 0.2-2.1 | Metal catalyst support; anticancer agent | 50,51 |
| Calf histone | Graphene | Tip sonication | -- | -- | 51 |
| Gelatin | Graphene, h-BN | Bath/tip sonication | 0.6-1.4 | Gelatin-based composites: mechanical reinforcement; gas barrier | 55,57 |
| Amphiphilic peptides | Graphene | Bath sonication | 0.03 | -- | 65 |
| *Nucleotides, RNA, DNA* | | | | | |
| Flavin mononucleotide | Graphene | Bath/tip sonication; electrochemical intercalation | 0.2-50 | Metal catalyst support for ORR and nitroarene reduction; support for cellular growth | 67–69 |
| RNA | Graphene | Bath sonication | -- | Transparent conducting films | 81 |
| DNA | Graphene, $WS_2$, $WSe_2$ | Bath/tip sonication | 0.8-2.3 | Anticancer and antibacterial agents | 80,82,83 |
| *Polysaccharides, plant extracts* | | | | | |
| Cellulose | Graphene, $MoS_2$, h-BN | Bath/tip sonication | 0.9–1.1 | Mechanical reinforcement in polymer composites, Na-ion batteries anode | 88–90 |
| Lignin | Graphene, $MoS_2$ | Bath/tip sonication | 0.65–13.5 | Mechanical reinforcement in polymer composites, Li-ion batteries cathode | 97–99 |
| Gum arabic | Graphene | Bath sonication | 0.69–1.12 | Mechanical reinforcement in polymer composites, metal catalyst support for SERS | 101–103 |
| Chitosan | Graphene, $MoS_2$ | Bath/tip sonication; ionic liquid–assisted grinding; oleum | 0.85–5.5 | Mechanical reinforcement and flame retardant in in polymer composites, NIR agent for photothermal ablation of cancer, chemotherapeutic drug | 108–113 |

| | | | | | |
|---|---|---|---|---|---|
| | | treatment | | nanocarrier for NIR–photothermal triggered drug delivery | |
| Hyaluronic acid | Graphene, $MoS_2$, h-BN | Tip sonication | -- | -- | 114 |
| Pullulan | Graphene | Tip sonication | 2.3 | -- | 108 |
| Guar gum | $MoS_2$ | Bath sonication | 0.24 | Metal catalysts support for nitroarene reduction | 115 |
| Xantham gum | $MoS_2$ | Tip sonication | 0.06 | Metal catalysts support for nitroarene reduction | 115 |
| Tannic acid | $MoS_2$ | Bath sonication | 0.15 | Metal catalysts support for nitroarene reduction | 115 |
| Levulinic acid | Graphene | Bath sonication | 0.065 | -- | 94 |
| Artemisia princeps | Graphene | Bath sonication | -- | -- | 116 |
| Xanthium strumarium | Graphene | Bath sonication | -- | -- | 116 |
| *Bile salts* | | | | | |
| Sodium cholate | Graphene, $MoS_2$, $MoSe_2$, $MoTe_2$, $WS_2$,$WSe_2$,$WTe_2$, $NbSe_2$, $TaSe_2$, h-BN, $MnO_2$ | Bath/tip sonication, shear mixing | 0.04-0.8 | Transparent conducting films; HER electrocatalyts; thermoelectric devices; Li-ion battery cathodes; mechanical reinforcement of polymer composites | 36,121-124,126-130,132, 134, 136 |
| Sodium deoxycholate | Graphene | Bath sonication | 0.1-2.6 | -- | 35,132 |
| Sodium taurodeoxycholate | Graphene | Bath/tip sonication | 0.02-12 | Metal catalyst support for ORR | 35,131 |
| CHAPS | Graphene | Bath sonication | 0.08 | -- | 35 |
| *Other bio-related compounds* | | | | | |
| Saccharin | Graphene | Electrochemical intercalation | -- | -- | 137 |
| Lecithin (phospholipid) | Graphene | Bath sonication | 0.05 | -- | 139 |
| POPC (phospholipid) | Graphene | Bath sonication | 0.1-0.2 | Antibacterial agent | 140 |
| Urea | Graphene, h-BN | Tip sonication, solid-state ball milling | 0.15-30 | -- | 141,142 |
| Amphotericin B (drug molecule) | Graphene | Solid-state ball milling | 0.15 | -- | 143 |
| Chlorin e6 (photosensitizer drug) | Graphene | Bath sonication | -- | Drug carrier for PDT | 144 |

Acronym definitions: photothermal therapy (PTT), photodynamic therapy (PDT), computed tomography (CT), oxygen reduction reaction (ORR), surface–enhanced Raman spectroscopy (SERS), near–infrared (NIR), hydrogen evolution reaction (HER), 3-[(3-cholamidopropyl)dimethyl ammonio]-1-propanesulfonate (CHAPS), 1–palmitoyl–2-oleoyl–*sn*–glycerol–3-phosphocholine (POPC).

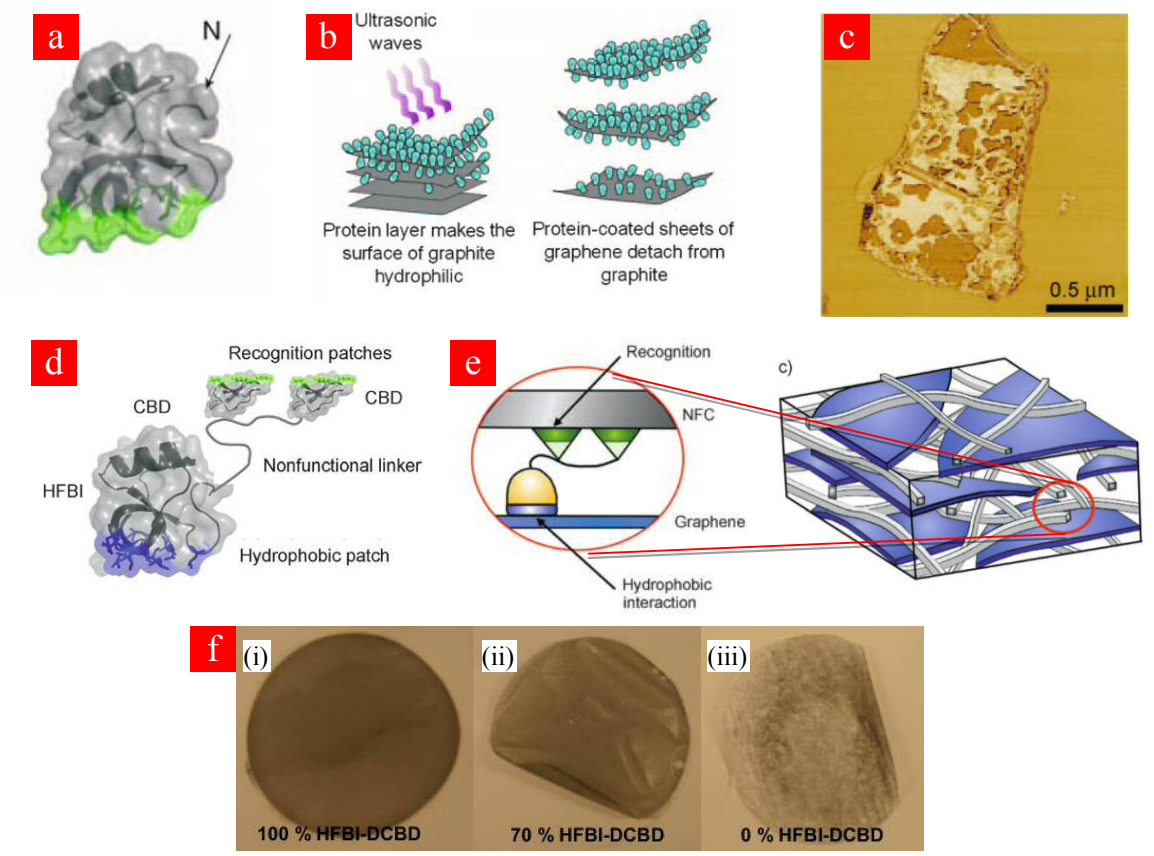


**Figure 1.** Use of hydrophobins towards the exfoliation of graphene in aqueous medium and preparation of graphene-based functional composites. (a) Schematic structure of the HFBI protein, which has a diameter of about 2 nm. The green area represents the patch of hydrophobic residues through which the protein adsorbs onto the graphene flakes. *N* denotes the N terminus of the molecule that is used as a chemical handle to attach additional species (e.g., proteins, peptides, etc) and generate HFBI variants. (b) The HFBI proteins adsorb onto the surface of graphite (left picture) to assist in its ultrasonic exfoliation to give HFBI-stabilized graphene flakes in water (right). (c) Atomic force microscopy image of an HFBI-exfoliated graphene flake showing an incomplete monolayer of adsorbed proteins in a lighter contrast. (d) Schematic structure of the HFBI-DCBD fusion protein, formed by two cellulose-binding domain (CDB) proteins appended to HFBI. The surface region of the CBD protein that binds selectively to cellulose is highlighted in green. (e) Schematic of the dual binding of HFBI-DCBD to nanofibrillated cellulose (NFC) and graphene (left picture), as well as the resulting, intimately mixed NFC-graphene composite (right). Graphene flakes are shown in cyan and NFC fibrils in gray color. (f) Digital photographs of NFC-graphene composite films prepared only with HFBI-DCBD (i), 70% HBFI-DCBD and 30% HFBI (ii) and only HFBI (iii). Reproduced from refs. 46 and 47 with permission from Wiley-VCH.

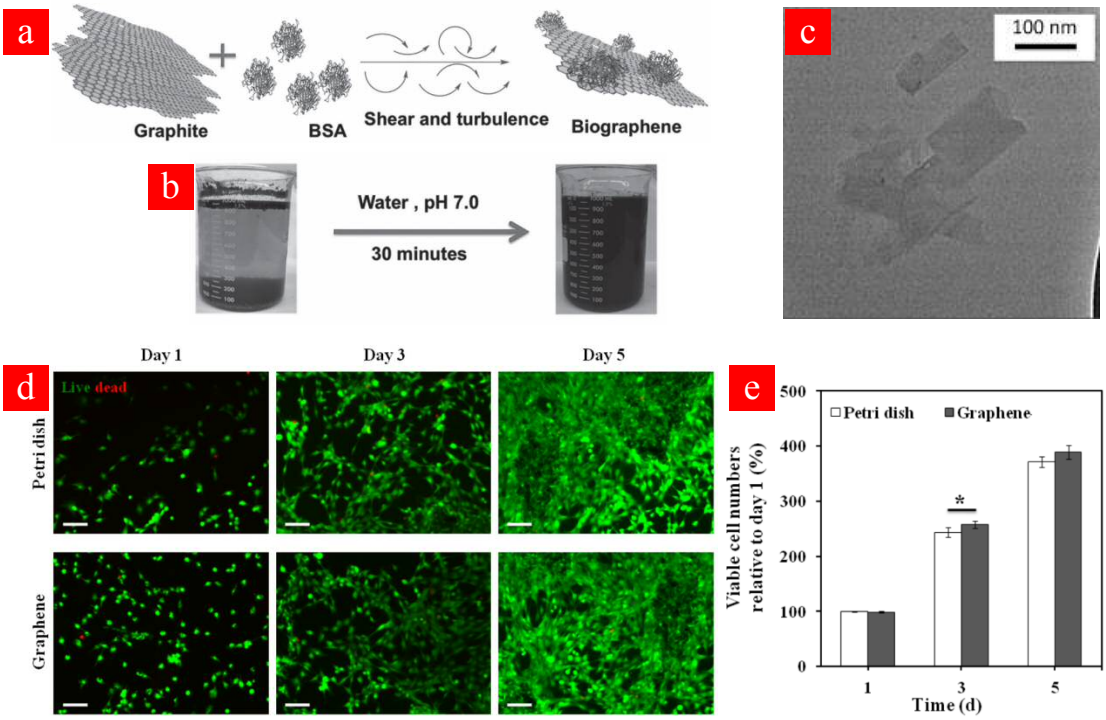


**Figure 2.** (a) Schematic of the exfoliation of graphite under shear forces using BSA as a dispersant. The resulting BSA-coated graphene flakes are referred to as biographene. (b) Digital photographs of graphite powder floating on an aqueous BSA solution before shear treatment (left beaker) and the resulting BSA-stabilized graphene dispersion after exfoliation (right beaker). (c) Transmission electron microscopy image of BSA-exfoliated few-layer graphene flakes. (d) Live/dead assay based on fluorescence images of C2C12 mouse myoblasts seeded at an initial density of $2\times10^4$ cells $cm^{-2}$ on a naked Petri dish (top row) and on a Petri dish covered with BSA-coated graphene flakes (bottom row). Green (red) indicates live (dead) cells. (e) Quantification of viable C2C12 myoblasts 1, 3 and 5 days after cell seeding on both naked and BSA-stabilized graphene-covered Petri dishes. Reproduced from refs. 52 and 53 with permission from Wiley-VCH and Royal Society of Chemistry, respectively.

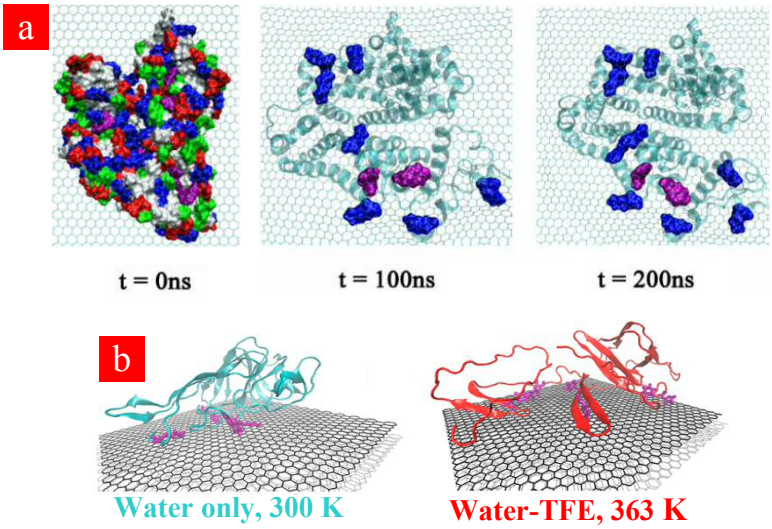


**Figure 3.** Simulation of the adsorption of proteins onto the graphene surface. (a) Three representative snapshots at t = 0, 100 and 200 ns from a MD simulation of the interaction of BSA with graphene in the presence of water molecules (not shown). In the initial, non-interacting configuration (t = 0 ns), the basic, acidic, aromatic as well as other hydrophobic and hydrophilic residues are highlighted in blue, red, purple, white and green respectively. Following BSA adsorption, only the residues that are interacting with the graphene surface are highlighted, which reveals the important role of basic residues. (b) MD simulation snapshots of the interaction of soy protein and graphene in water at 300 K (left) and in water-trifluoroethanol (TFE) mixture at 363 K (denaturated protein, right). The number of aromatic groups interacting with graphene (highlighted in purple) increases from ~3 to about ~6 when the protein becomes denaturated. Reproduced from refs. 59 and 64 with permission from Nature Publishing Group and American Chemical Society, respectively.

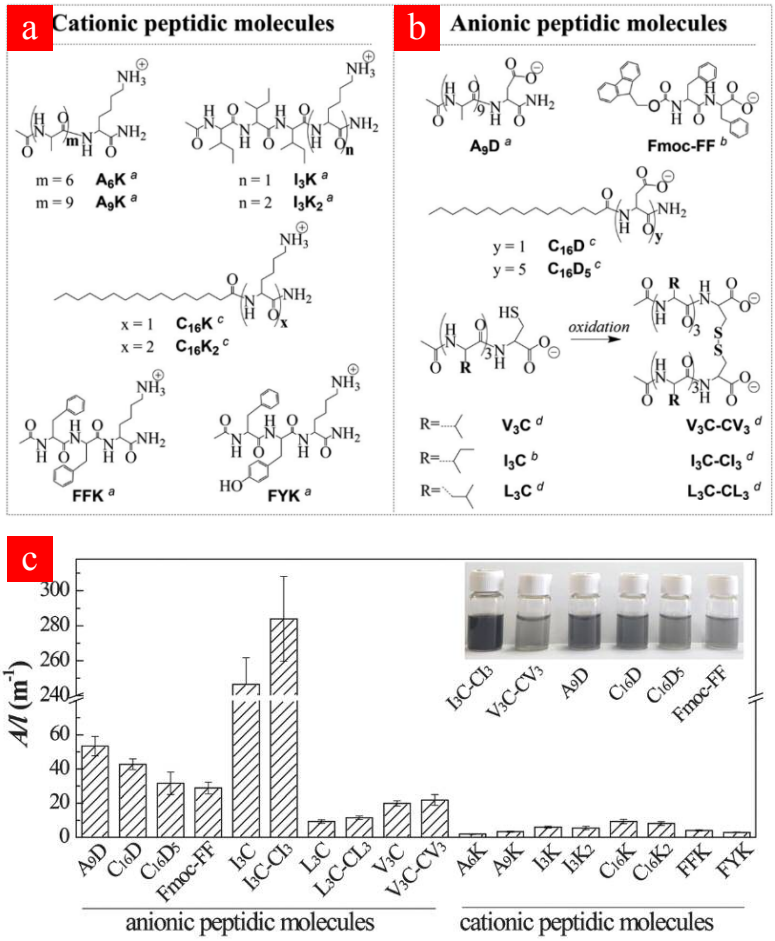


**Figure 4.** Use of peptides in the exfoliation and dispersion of graphene in water. (a,b) Molecular structure of the tested cationic (a) and anionic (b) peptides. The capital letters denote specific amino acids or alkyl chains: alanine (A), lysine (K), isoleucine (I), phenylalanine (F), tyrosine (Y), aspartic acid (D), valine (V), cysteine (C), leucine (L) and hexadecyl chain ($C_{16}$). The gemini surfactant-like peptides (e.g., $V_3C$-$CV_3$) were generated by oxidation of the thiol group in the cysteine residue of the monomeric peptide and subsequent formation of disulfide bridges. (c) Comparison of relative concentrations for graphene dispersions obtained with the different peptides. *A/l* denotes the optical absorbance (per unit path length) of the graphene suspensions measured at a wavelength of 660 nm, which is proportional to the suspension concentration according to the Lambert-Beer law. Inset: digital photograph of a representative set of aqueous graphene dispersions. Reproduced from ref. 65 with permission from Royal Society of Chemistry.

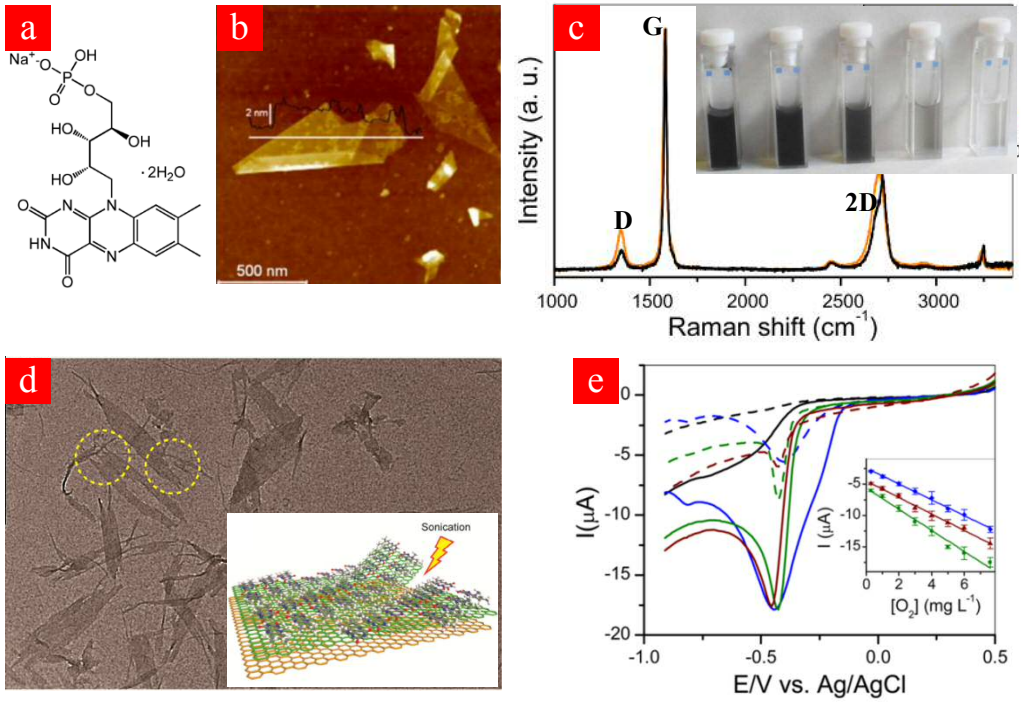


**Figure 5.** (a) Chemical structure of flavin mononucleotide (FMN). (b) Atomic force microcopy image of FMN-exfoliated graphene flakes. The flakes are submicrometric in lateral size and a few nanometers thick. (c) Raman spectra of FMN-exfoliated graphene (orange trace) and the starting graphite powder (black). A low D to G band ratio denotes high quality graphene flakes. Inset: digital photograph of cuvettes containing (from left to right) a concentrated (~45 mg $mL^{-1}$) FMN-stabilized graphene dispersion, the same dispersion diluted by a factor of 100, 1000 and 5000, as well as pure water. (d) Transmission electron microscopy image of graphene nanoribbons obtained from FMN-templated unzipping of graphene flakes. Inset: schematic of the templating process. (e) Linear scan voltammograms of $O_2$ reduction at glassy carbon electrodes modified with FMN-stabilized graphene-metal NP hybrids in $O_2$- and $N_2$-saturated 0.2 M NaOH solution (solid and dotted lines, respectively). The studied materials were graphene only (black), graphene-Pt NP hybrid (blue), graphene-Pd NP hybrid prepared in ethanol (green) and graphene-Pd NP hybrid prepared with $NaBH_4$ (brown). Scan rate: 50 mV $s^{-1}$. The inset shows the corresponding $O_2$ concentration calibration curves. Reproduced from refs. 67 and 68 with permission from American Chemical Society and Elsevier, respectively.

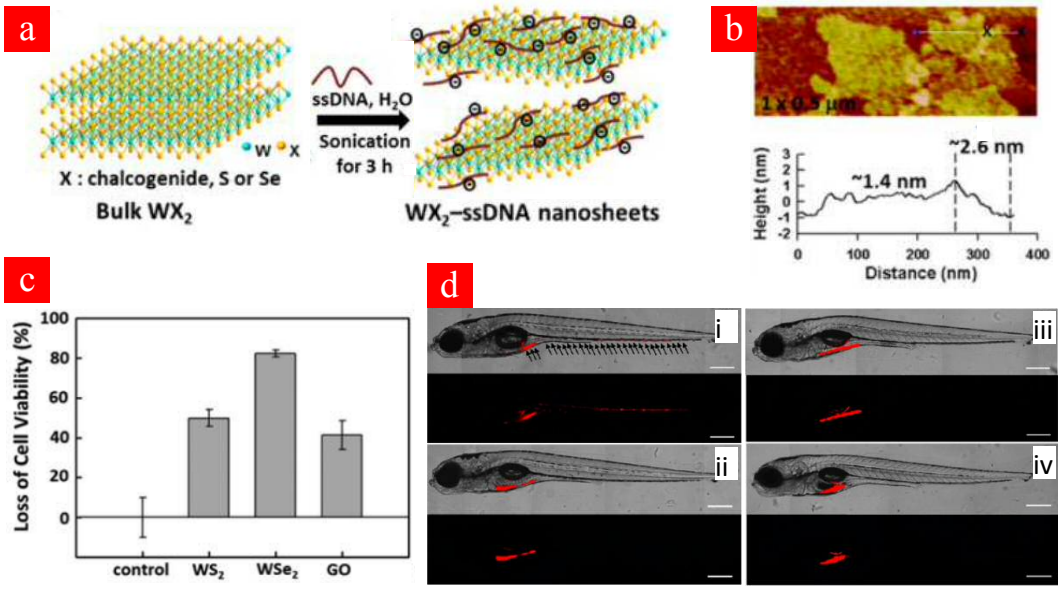


**Figure 6.** (a) Schematic of the exfoliation of bulk $WS_2$/$WSe_2$ with ssDNA in water via sonication to give single-/few-layer flakes of these TMDs. The ssDNA-stabilized flakes are negatively charged due to the phosphate groups of ssDNA. (b) Atomic force microscopy image (top) and line profile (bottom) of ssDNA-exfoliated $WS_2$ flakes. (c) Viability loss of *Escherichia coli* cells upon exposure for 5 h to an aqueous dispersion of ssDNA-exfoliated $WS_2$ or $WSe_2$ flakes (80 μg $mL^{-1}$). Results obtained with graphene oxide (GO) are also shown for comparison. (d) Representative fluorescence (dark background) and combined optical/fluorescence (light background) microscopy images revealing the migration of human colorectal cancer cells (HCT-116 line) xenografted on the yolk sac of zebrafish embryos: (i) control group (no drug), (ii) with addition of 50 nM paclitaxel, (iii) 50 μg $mL^{-1}$ and (iv) 75 μg $mL^{-1}$ dsDNA-exfoliated graphene. The arrows in (i) indicate tumor foci disseminated from the yolk sac. Reproduced from refs. 82 and 83 with permission from American Chemical Society.

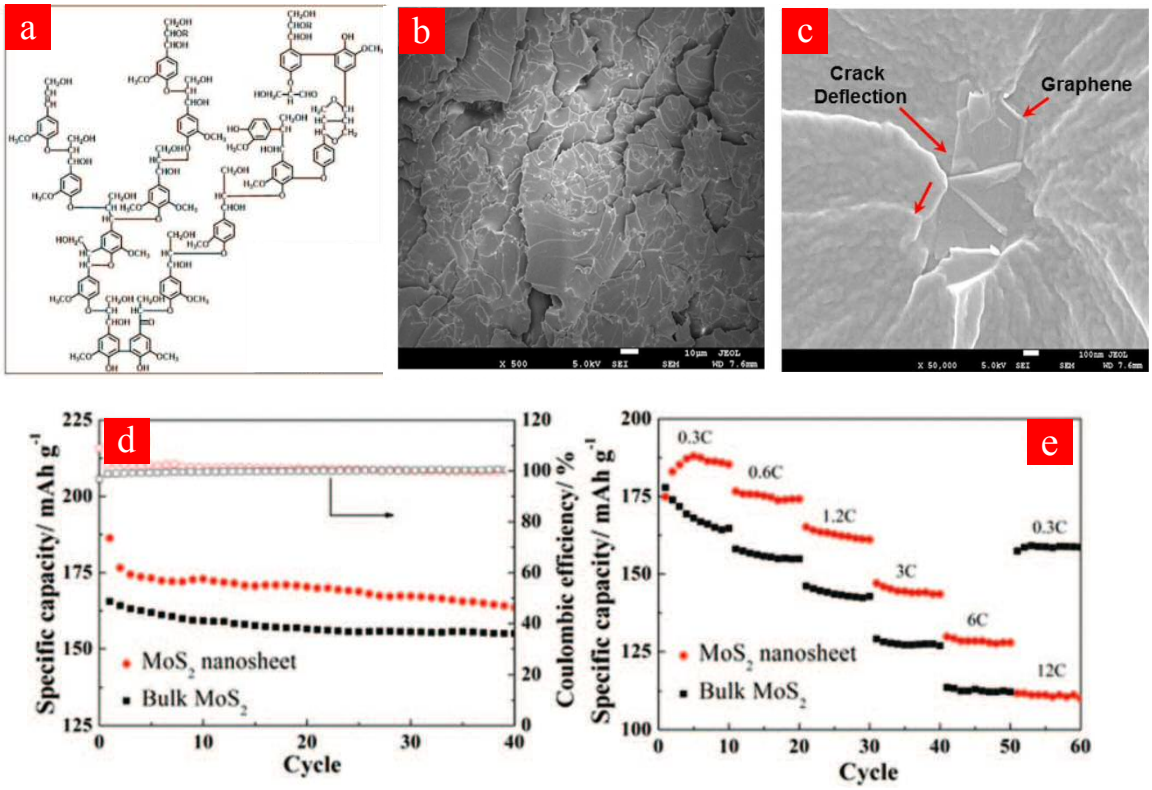


**Figure 7.** Use of alkali lignin (AL) as a green dispersant for 2D materials. (a) Structural model of lignin. (b,c) Scanning electron microscopy images of fractured surfaces of epoxy/AL-exfoliated graphene composites with 0.1 wt% graphene loading. The scale bars in (b) and (c) are 10 μm and 100 nm, respectively. (d) Cycling performance at 0.6 C and (e) rate capabilities (1-3 V range) of AL-exfoliated $MoS_2$ flakes in tests as a cathode for Li-ion batteries. Reproduced from refs. 98 and 99 with permission from Elsevier and Royal Society of Chemistry, respectively.

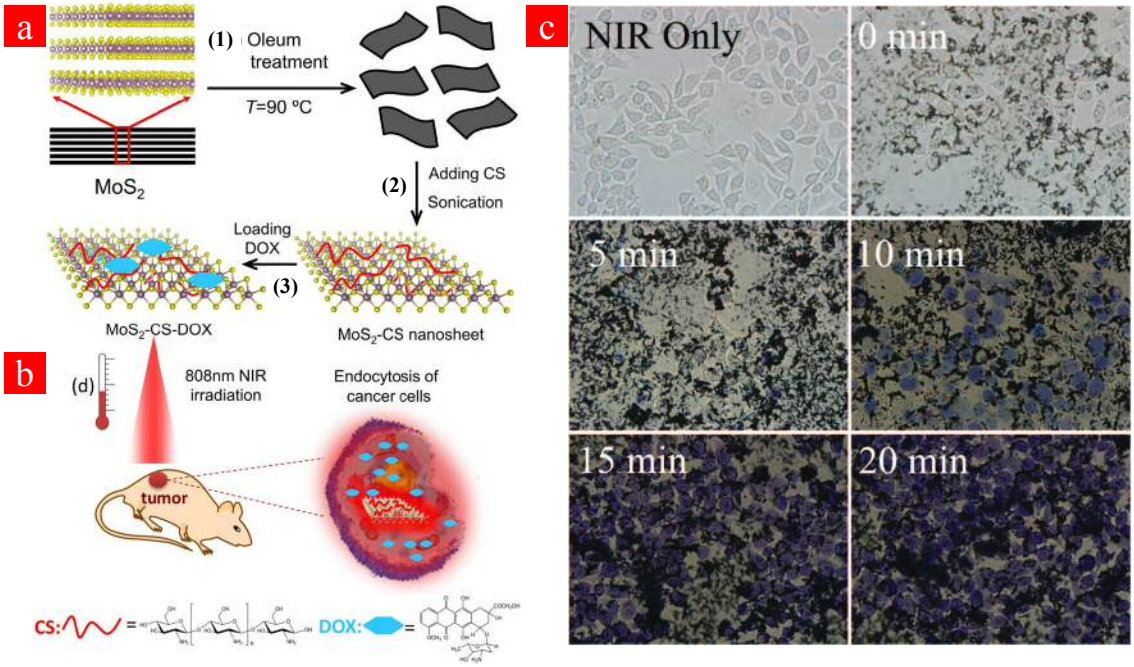


**Figure 8.** Chitosan (CS)-modified $MoS_2$ flakes as a NIR light–triggered drug delivery system for cancer therapy. (a) Schematic illustration of the synthesis of the CS-modified $MoS_2$ ($MoS_2$–CS) flakes: (1) exfoliation by oleum treatment to produce single-layer $MoS_2$ flakes, (2) subsequent modification with CS and (3) loading of doxorubicin (DOX). (b) NIR light–triggered delivery of DOX loaded onto the $MoS_2$ flakes to the tumor site. (c) Optical microscopy images of the photothermal destruction of human hepatocyte carcinoma (HepG2) cells incubated with 50 μg $mL^{-1}$ $MoS_2$-CS flakes following different times of exposure to 808 nm NIR light irradiation at a power of 2 W $cm^{-2}$. Because they can be readily stained by trypan blue, the dead cells emerge as blue spots in the images. Reproduced from refs. 112 and 113 with permission from American Chemical Society and Royal Society of Chemistry, respectively.

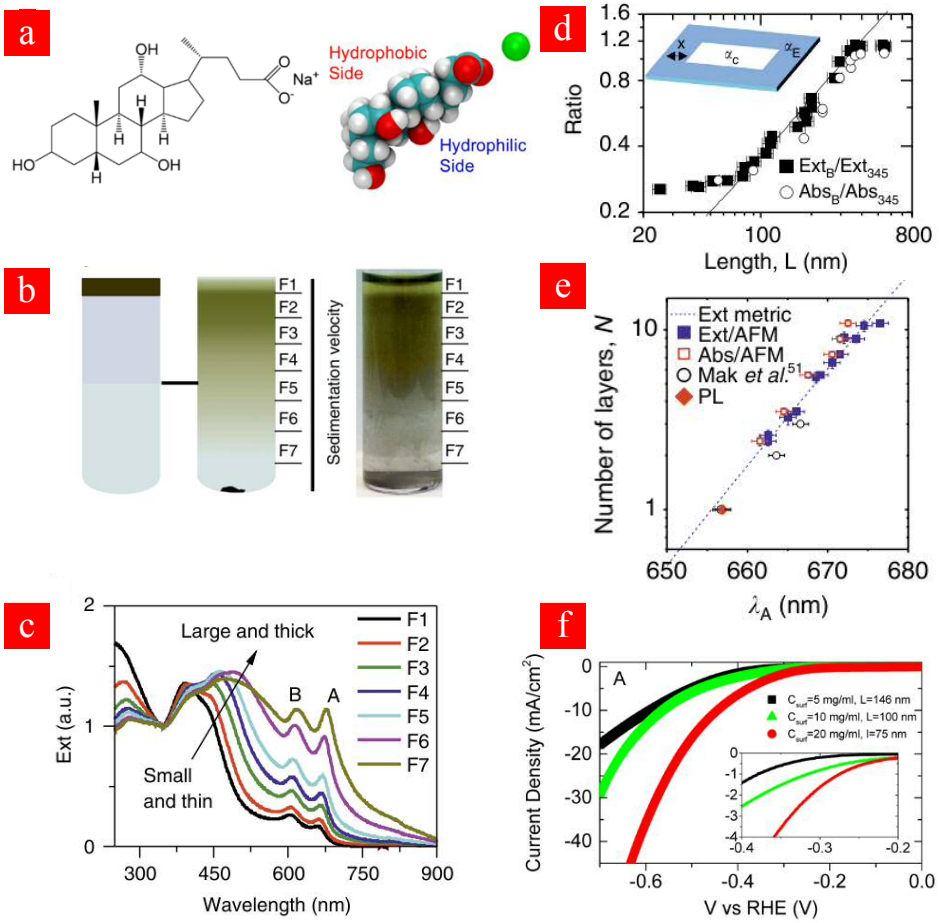


**Figure 9.** Preparation and use of bile salt-exfoliated $MoS_2$. (a) Left: chemical structure of sodium cholate (SC). Right: all-atom molecular model of SC (red: O; cyan: C; green: Na; white: H). (b) Sorting of SC-exfoliated $MoS_2$ flakes via band sedimentation centrifugation. Schematic of the experimental setup: a stock $MoS_2$ dispersion is layered on top of a race layer containing $D_2O$ and a 1:1 mixture of $D_2O$ and $H_2O$ (left); after centrifugation, seven fractions are separated along the race layer (middle); a digital photograph of a dispersion after band sedimentation (right). (c) Extinction spectra of the fractions normalized to the local minimum at 345 nm. (d) Ratio of extinction at B-exciton to local minimum at 345 nm, $Ext_B/Ext_{345}$, plotted as a function of mean flake length, L, measured by transmission electron microscopy. (e) Mean number of monolayers per flake (measured from atomic force microscopy images) plotted against the position of the A-exciton peak observed in extinction and absorbance spectra. The data for both extinction and absorbance are very similar. (f) Linear sweep voltammograms (5 mV $s^{-1}$) recorded for thin films of SC-exfoliated $MoS_2$ flakes deposited onto pyrolytic carbon substrates, revealing their electrocatalytic response towards HER. Data for $MoS_2$ samples with mean flake length of 146 nm (black line), 100 nm (green) and 75 nm (red) are shown. Reproduced from refs. 119, 127 and 130 with permission from American Chemical Society and Nature Publishing Group.

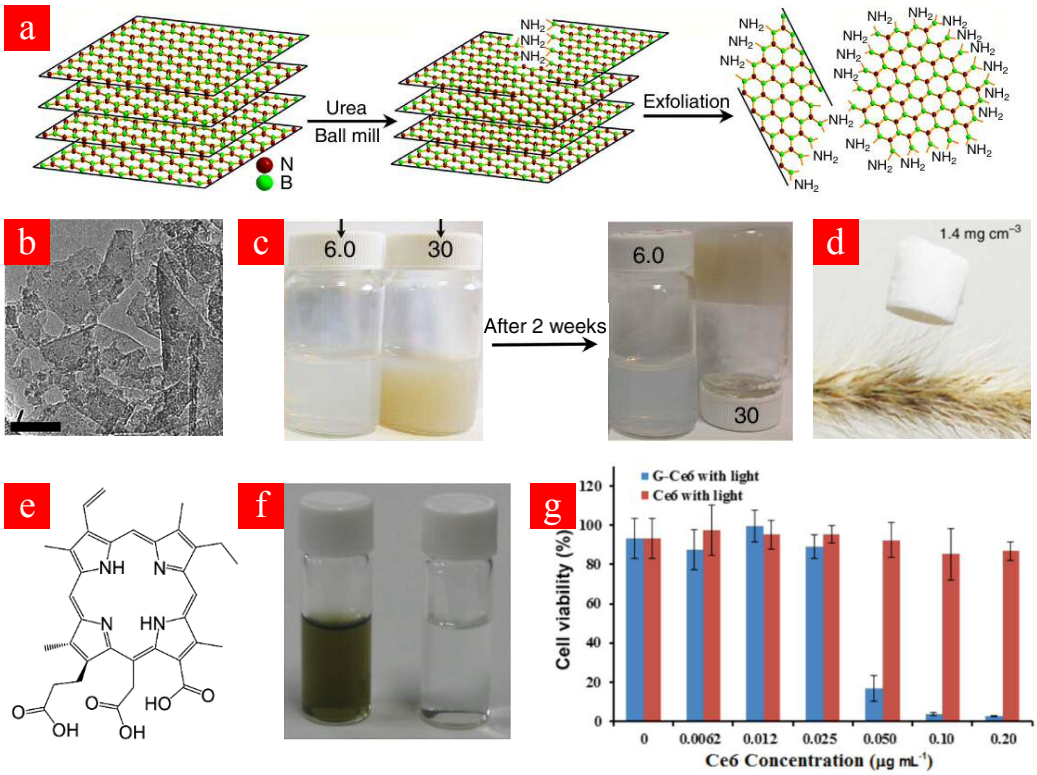


**Figure 10.** (a) Schematic of the exfoliation of h-BN with urea by a solid-state ball milling approach. (b) Transmission electron microscopy image of urea-exfoliated h-BN flakes (scale bar: 50 nm). (c) Left photograph: as-prepared, urea-exfoliated aqueous h-BN dispersions at concentrations of 6 and 30 mg mL$^{-1}$. Right photograph: same dispersions after standing undisturbed for two weeks. Gelling is observed for the highly concentrated dispersion (d) Digital photograph of an h-BN aerogel obtained after freeze-drying a gelled dispersion. (e) Chemical structure of chlorin e6. (f) Digital photograph of the supernatant obtained after sonication and centrifugation of graphite in the presence (left) and absence (right) of chlorin e6. (g) Cell viability of HeLa cells exposed to either graphene-chlorin e6 hybrid (G-Ce6) or to free chlorin e6 (Ce6) and irradiated with 660 nm laser light for 2 min. Reproduced from refs. 142 and 144 with permission from Nature Publishing Group and American Chemical Society, respectively.